Published in final edited form as:
Neuroscience. 2012 May 17; 210: 451–466. doi:10.1016/j.neuroscience.2012.02.038.

Prevention of posttraumatic axon sprouting by blocking CRMP2-mediated neurite outgrowth and tubulin polymerization

Sarah M. Wilson[1], **Wenhui Xiong**[1,2,5], **Yuying Wang**[3], **Xingjie Ping**[1,2,5], **Jessica D. Head**[4], **Joel M. Brittain**[1], **Pravin D. Gagare**[#], **P. Veeraraghavan Ramachandran**[#], **Xiaoming Jin**[1,2,5,*], and **Rajesh Khanna**[1,3,5,*]

[1]Stark Neurosciences Research Institute, Indiana University School of Medicine, Indianapolis, IN 46202, USA

[2]Department of Anatomy and Cell Biology, Indiana University School of Medicine, Indianapolis, IN 46202, USA

[3]Department of Pharmacology and Toxicology, Indiana University School of Medicine, Indianapolis, IN 46202, USA

[4]Indiana University Purdue University Indianapolis, Indiana University School of Medicine, Indianapolis, IN 46202, USA

[5]Indiana Spinal Cord and Brain Injury Research Group, Indiana University School of Medicine, Indianapolis, IN 46202, USA

[#]Department of Chemistry, 560 Oval Drive, Purdue University, West Lafayette, Indiana 47907-2084

Abstract

Epileptogenesis following traumatic brain injury (TBI) is likely due to a combination of increased excitability, disinhibition, and increased excitatory connectivity via aberrant axon sprouting. Targeting these pathways could be beneficial in the prevention and treatment of posttraumatic epilepsy. Here, we tested this possibility using the novel anticonvulsant (*R*)-*N*-benzyl 2-acetamido-3-methoxypropionamide ((*R*)-lacosamide (LCM) which acts on both voltage-gated sodium channels and collapsin response mediator protein 2 (CRMP2), an axonal growth/guidance protein. LCM inhibited CRMP2-mediated neurite outgrowth, an effect phenocopied by CRMP2 knockdown. Mutation of LCM binding sites in CRMP2 reduced the neurite inhibitory effect of LCM by ~8-fold. LCM also reduced CRMP2-mediated tubulin polymerization. Thus, LCM selectively impairs CRMP2-mediated microtubule polymerization which underlies its neurite outgrowth and branching. To determine whether LCM inhibits axon sprouting *in vivo*, LCM was injected into rats subjected to partial cortical isolation, an animal model of posttraumatic epileptogenesis that exhibits axon sprouting in cortical pyramidal neurons. Two weeks following injury, excitatory synaptic connectivity of cortical layer V pyramidal neurons was mapped using patch clamp recordings and laser scanning photostimulation of caged glutamate. In comparison to injured control animals, there was a significant decrease in the map size of excitatory synaptic

[*]**Co-corresponding Authors: Xiaoming Jin, Ph.D.**, 980 W. Walnut St., R3 Room C426B, Indianapolis, IN 46202, USA. Office: (317) 278-5766; Fax: (317) 278-5849 xijin@iupui.edu or **Rajesh Khanna, Ph.D.,** 950 W. Walnut St., R2 Room 478, Indianapolis, Indiana 46202, USA. Office: (317) 278-6531; Fax: (317) 278-5849 khanna5@iupui.edu.

connectivity in LCM-treated rats, suggesting that LCM treatment prevented enhanced excitatory synaptic connectivity due to posttraumatic axon sprouting. These findings suggest, for the first time, that LCM's mode of action involves interactions with CRMP2 to inhibit posttraumatic axon sprouting.

Keywords

Epileptogenesis; Posttraumatic sprouting; CRMP2; Neurite outgrowth; Sholl analysis; Tubulin polymerization; Lacosamide

Introduction

Traumatic brain injury (TBI) affects millions of people in the United States each year (Granacher, 2003). Aside from immediate challenges of the insult, one of the more common complications associated with TBI is the development of posttraumatic epilepsy (PTE; (Diaz-Arrastia et al., 2009). The latency between the time of injury and onset of seizure activity, which can range from weeks to years, may allow for prophylactic intervention to prevent epileptogenesis (Prince et al., 2009). However, classical antiepileptic drugs (AEDs) such as phenytoin, phenobarbital, carbamazepine, and valproate failed clinical trials for the prevention of PTE (Temkin, 2009). Animal models of PTE have revealed significant morphological changes occurring during the latency period which may be attributed to the development of epileptiform activity. One of the more striking changes is aberrant sprouting of axons in response to injury, which has been observed both in the hippocampus and the neocortex in a variety of PTE models (Salin et al., 1995; Golarai et al., 2001; Kharatishvili et al., 2006). Sprouting of injured axon fibers may account for the increased excitatory connectivity observed in a neocortical isolation model of PTE (Jin et al., 2006). The ability to target sprouting as well as other maladaptive processes occurring during the latency period may aid in the prevention of posttraumatic epileptogenesis.

Recently, lacosamide ((R)-*N*-benzyl 2-acetamido-3-methoxypropionamide (LCM)), a modulator of voltage-gated sodium channels, was approved as a novel anticonvulsant (Choi et al., 1996; Perucca et al., 2008; Curia et al., 2009; Harris and Murphy, 2009; Kelemen and Halasz, 2010). The action of lacosamide is unique in that it retains the ability to selectively enhance slow inactivation of sodium channels without affecting fast inactivation (Errington et al., 2008; Sheets et al., 2008). However, a second target has been identified for LCM, the collapsin response mediator protein 2 (CRMP2) (Beyreuther et al., 2007; Park et al., 2009). Kohn and colleagues (Park et al., 2009), using an affinity bait/chemical reporter derivatized LCM, showed biochemical binding to CRMP2 but did not address the mechanism by which LCM's interaction with CRMP2 affects the protein's canonical functions.

CRMP2 is an intracellular phosphoprotein involved in axon guidance and neurite outgrowth (Wang and Strittmatter, 1996; Schmidt and Strittmatter, 2007). CRMP2 is phosphorylated in response to semaphorin3A signaling, rendering it unable to promote neurite outgrowth (Schmidt and Strittmatter, 2007). Central to CRMP2's role in neurite dynamics is its ability to promote microtubule assembly by binding tubulin dimers (Fukata et al., 2002; Kimura et al., 2005). Additionally, CRMP2 mediates microtubule polymerization by enhancing tubulin's GTPase activity (Chae et al., 2009). Overexpression of CRMP2 in cultured cortical neurons leads to the elongation and formation of processes (Inagaki et al., 2001). These properties identify CRMP2 as a potential candidate in targeting TBI-induced axon sprouting.

In this study, we investigated the effects of LCM's interaction with CRMP2 on CRMP2's function and on axonal sprouting in an animal model of posttraumatic epileptogenesis. Our

results demonstrate that LCM, at subtherapeutic concentrations (<40 μM (Greenaway et al., 2010)), selectively impairs CRMP2-mediated microtubule polymerization which underlies neurite outgrowth and branching. Importantly, LCM treatment during the latent period following injury attenuated increased excitatory connectivity *in vivo*.

Experimental Procedures

Chemicals and Solutions

All reagents were purchased from Sigma (St. Louis, MO) unless otherwise indicated. Lacosamide (*R*-2-acetamido-*N*-benzyl-3-methoxypropionamide) was purchased from Cayman Chemicals (Ann Arbor, MI) or synthesized as described (Choi et al., 1996) at Purdue University. A 100 mM solution was made up in N-Methylpyrrolidone (MPL) or dimethylsulfoxide (DMSO) and stored in small aliquots at −20°C. The final concentration of MPL in physiological solutions was less than 0.1% (v/v). A concentration of 300 μM was used because this represents about 3 times the value at which LCM shows anti-convulsant effects in in vitro studies (Lees et al., 2006) and approximately 5-fold the reported value for half-maximal inhibition of spontaneous excitatory postsynaptic currents and inhibitory postsynaptic current (Errington et al., 2006).

Primary Cortical and Hippocampal Neuronal Cultures

Primary cortical or hippocampal neurons were prepared from embryonic day 18–19 Sprague-Dawley rats as described (Wang et al., 2010a) with some modifications. Briefly, cortices or hippocampi were dissected and cell suspensions were plated onto poly-D Lysine-coated glass coverslips. Cells were grown in media consisting of Neurobasal medium containing 2% NuSerum, 5% NS21, supplemented with penicillin/streptomycin (100 U/ml; 50 μg/ml), 0.1 mM L-Glutamine and 0.4 mM L-glutamax (Invitrogen). 5-fluor-2′-deoxyuridine (1.5 μg/mL) (Sigma) was added 48 h after plating to reduce the number of non-neuronal cells. After 4 d in culture and 2× each week thereon, half of the growth medium was replaced with medium without 5-fluor-2′-deoxyuridine. All procedures were in accordance with Institutional Animal Care and Use Committee of the Indiana University School of Medicine.

Whole-Cell Patch-Clamp Recordings

Whole-cell voltage recordings were performed at room temperature on primary cultured hippocampal neurons using an EPC 10 Amplifier (HEKA Electronics, Germany). Electrodes were pulled from thin-walled borosilicate glass capillaries (Warner Instruments, Hamden, CT) with a P-97 electrode puller (Sutter Instrument, Novato, CA) such that final electrode resistances were 2–3 MΩ when filled with internal solutions. The internal solution for recording Na^+ currents contained (in mM): 110 CsCl, 5 $MgSO_4$, 10 EGTA, 4 ATP Na_2-ATP, and 25 HEPES (pH 7.2, 290–310 mOsm/l). For recording Na^+ currents, the external solution contained (in mM): 100 NaCl, 10 tetraethylammonium chloride (TEA-Cl), 1 $CaCl_2$, 1 $CdCl_2$, 1 $MgCl_2$, 10 D-glucose, 4 4-AP, 0.1 $NiCl_2$, 10 HEPES (pH 7.3, 310–315 mOsm/l).

Whole-cell capacitance and series resistance were compensated with the amplifier. Series resistances compensation (70–80%) was routinely applied. Cells were considered only when the seal resistance was more than 1GΩ and the series resistance was less than 10 MΩ. Linear leak currents were digitally subtracted by P/4.

Data Acquisition and Analysis

Signals were filtered at 10 kHz and digitized at 10–20 kHz. Analysis was performed using Fitmaster and origin8.1 (OriginLab Corporation, MA, USA). For activation curves, conductance (G) through Na^+ channels was calculated using the equation $G = I/(V_m - V_{rev})$,

where V_{rev} is the reversal potential, V_m is the membrane potential at which the current was recorded, and I is the peak current. Activation and inactivation curves were fitted to a Boltzmann function $G/G_{max} = 1/\{1+\exp[(V-V_{50})/k]\}$, where G is the peak conductance, G_{max} is the fitted maximal G, V_{50} is the half-activation voltage, and k is the slope factor. Additional details of specific pulse protocols are described in the results text or figure legends. Lacosamide was applied onto the cells through a custom made Y-tube micro-perfusion system.

Neurite/Dendrite Outgrowth and Sholl Analysis of Dendritic Complexity

Neurite outgrowth of cortical neurons, transfected with enhanced green fluorescent protein (EGFP), CRMP2-EGFP, control siRNA + EGFP, Crmp2-siRNA + EGFP, or $CRMP2_{5ALA}$-EGFP (see following sections) and incubated in the presence of various concentrations of LCM or 0.01% DMSO (control), was assessed as previously described (Wang et al., 2010b). Sholl analysis was performed with ImageJ software using an automated Sholl analysis plug-in, in which the soma boundary is approximated by an ellipsoid, and dendrite intersections are assessed at radial distances from the soma. Transfection of EGFP into neurons allowed optical identification and unequivocal determination of their arborizations. No attempt was made to distinguish between axons and dendrites in the Sholl analysis. However, using immunocytochemistry with a dendritic marker, MAP2, dendrites could be selectively identified (*data not shown*). Images were acquired with a Nikon Eclipse 90i microscope by an experimenter (J.D.H.) blinded to transfection/drug conditions. Images were acquired across 3 separate culture wells.

Knockdown of CRMP2 Expression by siRNA

Validated short interfering RNAs (siRNAs) against the rat CRMP2 (5′-ACTCCTTCCTCGTGTACAT-3′) sequence (Nishimura et al., 2003) and controls (scrambled sequence with approximately the same percentage of GC but no sequence homology) were used for CRMP2 knockdown (Invitrogen) in cortical neurons as described (Chi et al., 2009; Brittain et al., 2009; Brittain et al., 2011a; Brittain et al., 2011b). Cells were incubated for 2 days with vector- or scramble siRNA (200 nM) and extent of knockdown was assessed via immunoblot analysis. As reported previously (Chi et al., 2009), we observed ~90% knockdown of CRMP-2 compared to scramble siRNA (*data not shown*).

Synaptic Bouton Size

Synaptic bouton size was determined as previously described (Brittain et al., 2009). Briefly, presynaptic terminals of cultured cortical neurons (7–8 DIV) were loaded with the fluorescent styryl dye N-(3-triethylammoniumpropyl)-4-(6-(4-(diethylamino)phenyl)hexatrienyl)pyridinium dibrodmide (FM4-64; 15 μM) by incubation in a depolarizing solution containing 90 mM KCl, 32 mM NaOH, 2mM $CaCl_2$, 2mM $MgCl_2$, 25mM Hepes, and 30mM Glucose (pH 7.3) for 1 min. Cells were then washed with Ca^{2+}-free solution with advasep-7 (200μM; Biotinium, Inc.) to quench dye not taken up by endocytosis. Nerve terminals were identified under a confocal microscope (Nikon Livescan SFC inverted microscope) using an oil-immersion CFI Plan APO VC x60 objective lens. Fluorescence of the FM4-64 dye was excited at 543nm and terminals capable of dye uptake were considered functional release sites. Bouton size was determined by outlining the fluorescent puncta in regions of interest (ROI) using NIS Elements software. The area of each ROI was then determined.

Glutamate Release

Glutamate release from cultured cortical neurons was determined as previously described (Wang et al., 2010). Briefly, cells were washed three times with a non-depolarizing Hepes

buffer. Following the third wash, 150 μl of each samples was collected and boiled for 5 min. Release was then stimulated by incubating cells in a depolarizing Hepes buffer (90 mM KCl), at which point 150 μl was collected and boiled. A second basal measurement was obtained by re-incubating in the non-depolarizing buffer. The glutamate remaining content was determined by incubating cells in the non-depolarizing buffer with 2% Triton X-100 (Sigma) to release intracellular glutamate. Total content was determined to be the sum of the basal, stimulate, second basal, and remaining samples. Glutamate content in each sample was determined using the Amplex Red glutamic acid/glutamate oxidase assay kit (Invitrogen), where L-glutamic acid is oxidized by glutamate oxidase to produce α-ketoglutarate, NH_2, and H_2O_2. The reaction between the Amplex Red reagent and H_2O_2 is catalyzed by horseradish peroxidase to generate fluorescent product resorufin. Fluorescence was measured in a Victor^2 V multilabel plate reader (PerkinElmer, Shelton, CT) via excitation at 530nm and emission at 590 nm and compared to a standard curve.

CRMP2 and CRMP2$_{5ALA}$ protein purification

A CRMP2-GST construct containing 5 amino acids in predicted LCM binding regions of CRMP2 mutated to alanine (CRMP2$_{5ALA}$-GST; Glu-360, Ser-363, Lys-418, Ile-420, and Pro-443) was generated by subcloning the mutation containing portion of CRMP2$_{5ALA}$-EGFP into wild type CRMP2-GST (using restriction enzymes *Rsr*II and *Bgl*II). Both wildtype and mutant recombinant proteins were expressed and purified as previously described (Brittain et al., 2009).

Co-immunoprecipitation and immunoblotting

Immunoprecipitations and immunblotting were performed as described (Chi et al., 2009; Brittain et al., 2009) using lysates prepared from postnatal day 1 rat brains. Antibody against CRMP2 was from Primm Biotech (Cambridge, MA), while the βIII-tubulin antibody was from Promega (Madison, WI).

Turbidimetric assay for tubulin polymerization

Polymerization of tubulin was performed as described previously (Chae et al., 2009) with the following modifications. Polymerization was performed in 0.1 M PEM buffer (80 mM PIPES, pH 6.9, 1 mM EGTA, and 1 mM $MgCl_2$ 1 mM GTP, and 2 mg/ml tubulin. CRMP2 proteins (0.2 μM) as well as 3 μM LCM or .01% DMSO were added to the samples and pipetted onto a 96-well plate at 37°C. Turbidity changes were assessed at 340 nm using a Viktor V3 spectrophotometer (Perkin Elmer). Taxol (10 μM) was used as a positive control as it has been shown to increase tubulin polymerization detected in turbidimetric assays (Carlier and Pantaloni, 1983).

Surgical procedure and lacosamide treatment

Partially isolated islands of neocortex (“undercuts”) were produced in 18 anesthetized rats at P21-23, using previously described techniques with modifications (Hoffman et al., 1994; Xiong et al., 2011). All experiments were performed according to protocols approved by the Institutional Animal Care and Use Committee of the Indiana University School of Medicine. Briefly, rats were anesthetized with ketamine (80 mg/kg, i.p.) and xylazine (Rompun, 8 mg/kg, i.p.) and mounted on a stereotaxic frame. Following scalp incision, a ~3×5 mm bone window on the center of the parietal bone of the left hemisphere was removed to expose the frontoparietal cortex, leaving the dura intact. We used a special surgical device, which consisted of a 30 gauge needle bent at a right angle 3–4 mm from the tip and passed through a 25 gauge guiding tube that was attached to a rectangular supporting plate (Xiong et al., 2011). The needle tip was inserted tangentially through the dura, just beneath the pial vessels, parasagittally 1–2 mm from the interhemispheric sulcus, and lowered to a depth of

~2 mm. The needle then was rotated 120–135° to produce a contiguous white matter lesion, elevated to a position just beneath the pia, and removed. The skull opening was then covered with sterile plastic wrap (Saran Wrap), and the skin was sutured.

LCM treatment started on the day after undercut surgery. In the treatment group, 100 mg/kg LCM was injected daily via tail vein for seven days. The control group received undercut surgery and saline injection for one week. All animals were allowed to recover for at least another week at the end of treatment before being used for in vitro experiment.

Brain slice preparation, field potential recording, patch clamp recording, and glutamate uncaging

Fourteen to twenty days after the undercut surgery, the rats were anesthetized with pentobarbital (55 mg/kg, i.p.) and decapitated. The brain was rapidly dissected out and placed in ice-cold (4°C) oxygenated slicing solution. The solution contained (in mM): 230 sucrose, 2.5 KCl, 1.25 NaH_2PO4, 10 $MgSO_47HO_2$, 10 glucose, 0.5 $CaCl_22H_2O$, and 26 $NaHCO_3$. Coronal slices (350 μm) were cut with a vibratome through the lesioned sensorimotor cortex. After 1 h incubation at 36°C in standard artificial cerebrospinal fluid (ACSF), slices were maintained at room temperature. The ACSF contained the following (in mM): 126 NaCl, 2.5 KCl, 1.25 NaH_2PO_4, 2 $CaCl_22H_2O$, 2 $MgSO_47H_2O$, 26 $NaHCO_3$, and 10 glucose, pH 7.4 when saturated with 95% O_2–5% CO_2.

For field potential recording, slices were transferred onto an interface chamber and partially submerged in regular oxygenated ACSF at room temperature. A glass pipette with ~1 MΩ resistance when filled with ACSF was placed next to the transcortical lesion region in layer V. A concentric bipolar electrode was inserted into the white matter or below the lower edge of the undercut in layer VI. Stimulating pulses consisted of 200 μs constant currents at 0.05 Hz, increasing progressively from 50 μA up to 1000 μA

For patch clamp recording, single slices were transferred to a recording chamber where they were minimally submerged in high divalent ACSF. The slice was imaged with a monochrome charge-coupled device (CCD) video camera (Cohu, San Diego, CA). Recording electrodes were pulled from borosilicate glass tubing (outer diameter, 1.5 mm) and had an impedance of 4–7 MΩ when filled with K-gluconate-based intracellular solution containing the following (in mM): 95 K-gluconate, 40 KCl, 5 EGTA, 0.2 CaCl22H2O, 10 HEPES, and 0.5% biocytin. The osmolarity of the pipette solutions was adjusted to 285–295 mOsm and pH to 7.3 with 1 M KOH. Patch-clamp recordings were made from layer V pyramidal cells in areas close to the lesioned cortex, using infrared video microscopy (Zeiss Axioskop; Carl Zeiss, Oberkochen, Germany) and a 63x water-immersion lens with differential interference contrast optics, and an Axopatch 200A amplifier (Molecular Devices, Foster City, CA). Access resistance was measured in voltage-clamp mode from responses to 5 mV depolarizing voltage pulses. Recordings with access resistance <20 MΩ and without significant changes (<25%) during the recording were used for data analysis. The responses were low-pass filtered at 2 kHz and recorded. EPSCs were measured at a holding potential of −70 mV.

We employed a setup for laser scanning photostimulation, which was similar to the one described previously (Jin et al., 2006). The microscope on a manually mobile stage was rigidly connected to a mobile platform. A Q-switched, intra-cavity tripled Nd:YVO4 UV laser (355nm, 300 mW, Explorer-355-300-P; Newport, Irvine, CA) and a periscope were aligned and installed on the platform, which allowed coincident longitudinal and horizontal displacements of the microscope and the laser unit. The UV laser beam was reflected by the periscope to mirror galvanometers (model 6210; Cambridge Technology, Cambridge, MA) controlled by scanning and data acquisition software. The laser beam passed through a lens

assembly, reflected by a dichroic mirror in the epifluorescence port of the microscope to the back aperture of a 5X objective.

For glutamate uncaging, the slice was submerged in 20 ml recirculating ACSF solution containing 100 μM MNI-glutamate and 50 μM APV (Both from Tocris, Ellisville, MO). Once a whole-cell recording was established, focal photolysis of caged glutamate was accomplished by switching the UV laser to give a 300–600 μs light stimulus. The duration of light stimulus was adjusted in each neuron so that the amplitude of direct activation on the soma was larger than 200 pA. The mapping stimulus patterns consisted of 18–22 rows and 10–11 columns with 50 μm spacing between adjacent spots, resulting in a 900–1100 × 500–550 μm mapping area in the slices. The grid was carefully aligned to cover cortical layers II–VI. We used a pseudo-random stimulus sequence pattern at a 3s interstimulus interval.

Slice electrophysiology – data analysis

In each recording trace corresponding to an uncaging site, all EPSCs occurring within a time window between ~7 ms and 100 ms after photostimulation were regarded as uncaging evoked responses. These events were detected using PSC detecting software (Jin et al., 2006; Jin et al., 2011) and added together to give a cumulative amplitude. This value was corrected for spontaneous EPSCs by subtracting a mean EPSC amplitude obtained by averaging prestimulus EPSPs over an equivalent time window in all traces of the map.

In each individual map, normalized EPSC amplitude for each row of stimulus spots, a comprehensive measurement reflecting the range and strength of synaptic connectivity with presynaptic neurons in the maps, were calculated by dividing the sum of EPSC amplitude of all spots in a row by the total number of stimulus sites in the row (Jin et al., 2006; Jin et al., 2011).

Mean hotspot amplitude in each row, which collectively indicated the strength of synaptic connection in the hotspots, was calculated by dividing the sum of EPSC amplitudes of all spots in a row by the total number of hotspots in the row; hotspot ratio in each row, positively proportional to the number of connected presynaptic neurons, was calculated by dividing the total number of spots in a row by the total number of hotspots in the row. Data from each treatment group were on the somata of the neurons and plotted along cortical depths to reveal possible differences in the strength and range in interlaminar cortical connectivity.

Statistical significance for group means was determined with two tailed Student’s t-test with $p<0.05$. Data are presented as mean ± SEM. Origin and Microsoft Excel software were used to perform all statistical analyses.

Results

Over-expression of CRMP2 blunts effect of lacosamide on sodium channels

Using the whole-cell patch clamp configuration, the potential effects of LCM on voltage-gated sodium channels (VGSCs) in the presence of over-expressed CRMP2 were examined. Recordings were obtained from hippocampal neurons grown for 7–10 days *in vitro* (DIV). In order to minimize space clamp complications caused by the extensive network of arborization present in these cultures, recordings were made from well-isolated cells. Current-voltage relationships in control (EGFP, enhanced green fluorescent protein) or CRMP2-EGFP expressing neurons were examined by the application of 20-ms step depolarizations ranging from −40 mV to + 60 mV (in 10 mV increments) from a holding potential of −100 mV. Peak inward Na^+ currents were measured and expressed as peak

current density (pA/pF) to account for variations in cell size. Representative peak Na^+ current traces from EGFP and CRMP2-EGFP–transfected neurons are shown in Figure 1A. EGFP-expressing neurons exhibited a peak current density of −150.9 ± 25.9 pA/pF (n=5), whereas CRMP2-EGFP–expressing neurons had a density of −140.3 ± 22.1 pA/pF (n=6; p >0.3). The endogenous Na^+ currents in control EGFP-expressing neurons were fully blocked by 500 nM TTX (*data not shown*). Application of 300 μM LCM to the clamped EGFP-expressing cells resulted in a reduction in peak Na^+ current observed at potentials between −30 and +40 mV (Figure 1C). Average normalized inhibition of peak Na^+ current by 300 μM LCM was ~61.8 ± 12.7% (n=5; Figure 1B). Inhibition of Na^+ currents was not accompanied by changes in voltage-dependence of activation gating for the channels (*data not shown*) (V_{50}: EGFP untreated, −21.5 ± 1.4 mV; k, 9.6 ± 0.91 mV, n=3; EGFP +LCM, −26.2 ± 1.1 mV; k, 9.7 ± 1.2 mV, n=3; p >0.05; Student's t-test). In contrast, in CRMP2-EGFP–overexpressing neurons, application of 300 μM LCM did not produce any appreciable Na^+ current inhibition (13.0 ± 8.1%, n=6; p <0.05, Student's t-test compared to LCM-mediated inhibition in EGFP neurons; Figure 1B). Voltage-dependence of activation gating in these neurons was not different from those expressing EGFP (V_{50}: CRMP2-EGFP untreated, −22.4 ± 2.2 mV; k, 5.6 ± 1.1 mV, n=4; CRMP2-EGFP +LCM, −22.9 ± 0.7 mV; k, 5.8 ± 0.6 mV, n=5; p >0.05).

LCM has been demonstrated to reduce VGSC availability by selectively enhancing the transition to a slow-inactivated state of VGSCs (Errington et al., 2008; Sheets et al., 2008). Since our data indicated that CRMP2 over-expression can significantly reduce the LCM-mediated inhibition of Na^+ currents, we tested the ability of LCM to bind to a slow-inactivated state in EGFP and CRMP2-EGFP overexpressing neurons. Transfected neurons were held at −70 mV, conditioned to potentials ranging from −120 mV to −10 mV (in 10 mV increments) for 5 s, and then fast-inactivated channels were allowed to recover for 1 s at a hyperpolarized pulse to −70 mV, and the fraction of channels available was tested by a single depolarizing pulse, to −10 mV, for 30 ms. The inactivation voltage curve was fit using a Boltzmann equation as described previously (Errington et al., 2008). In EGFP expressing neurons, LCM shifted the slow inactivation curves to more hyperpolarized membrane potentials (Figure 1C). The V_{50} for steady-state slow inactivation was −57.7 ± 3.8 mV (n=5) in LCM-treated EGFP expressing cells compared with −38.7 ± 6.5 mV (n=7) in untreated EGFP expressing cells (p < 0.05; Student's ttest; Figure 1C). In contrast, in cells overexpressing CRMP2-EGFP the V_{50} of slow inactivation was not affected by LCM (V_{50}: CRMP2-EGFP untreated, −35.8 ± 5.5 mV, n=5; CRMP2-EGFP +LCM, −37.9 ± 5.2 mV, n=5; p > 0.2; Figure 1C). The slopes (k) of the slow inactivation curves were not significantly different between all the groups tested (*data not shown*). Lacosamide may preferentially bind CRMP2 over the voltage-gated sodium channel, whereby excess amounts of CRMP2 prevent lacosamide from interacting with the channel. Collectively, these results suggest that over-expression of CRMP2 reduces the inhibitory effects of LCM on VGSCs.

Lacosamide blocks CRMP2-mediated neurite dynamics

While lacosamide may preferentially bind CRMP2, it is not known if it can alter the function of the CRMP2 protein. As CRMP2 is a positive regulator of neurite growth/dynamics, we tested the effect of 300 μM LCM on neurite complexity in CRMP2-overexpressing neurons. While this dose is well above the required dose for modulation of sodium channel function, it was chosen as a starting point as LCM's interaction with CRMP2 remains poorly classified. In order to assess the degree of neurite growth and branching we employed Sholl analysis on cortical neuron cultures overexpressing GFP or CRMP2-GFP. This technique measures the number of neurites crossing concentric circles (denoted as intersections or branch points) at various radial distances from the cell soma (Sholl, 1953). This consecutive-circles (cumulative intersection) analysis identifies dendritic

geometry, ramification abundance, and dendritic branching patterns. Cortical cultures were transfected with EGFP or CRMP2-EGFP at 9 DIV and analyzed 2 days following transfection. Consistent with its canonical role, overexpression of CRMP2-EGFP led to a significant increase in neurite complexity compared to GFP overexpression (Figure 2). In order to determine the effect of LCM on this phenomenon, 300 μM LCM was applied overnight to CRMP2-EGFP overexpressing cells 24 hours following transfection. Application of 300 μM LCM completely blocked the CRMP2-induced increase in neurite complexity (Figure 2B–C). To address the possibility that the observed reductions in neurite complexity were due to the effects of LCM on voltage-gated Na^+ channels, we repeated the morphological experiments in the presence of classical Na^+ channel blockers which do not target CRMP2 including carbamazepine (300 μM), lidocaine (200 μM), or tetrodotoxin (500 nM). No significant changes in neurite complexity were observed following these treatments (Figure 2C), suggesting the mechanism for the reduction in the CRMP2-mediated neurite branching is independent of LCM's effect on voltage-gated sodium channels.

To further characterize the effect of LCM on CRMP2-mediated neurite outgrowth, dose-response curves were completed in CRMP2-EGFP and EGFP over-expressing neurons. At 24 hours following transfection, varying doses of LCM were administered overnight and the effect on neurite branching/outgrowth was analyzed (Figure 3). IC_{50} values for inhibition of neurite complexity were obtained by comparing the number of intersections at ~275 μm from the soma, as this was the relative distance at which the number of intersections peaked. For neurons overexpressing CRMP2-EGFP, the IC_{50} of neurite inhibition was observed at 3.5±1.7 μM LCM (Figure 3B). In contrast, in cells overexpressing EGFP, the calculated IC_{50} was 25.7 ± 1.9 μM LCM (Figure 3D). While kinetic models predict that over-expression should not alter potency, the output measured in these experiments (neurite outgrowth/branching) is not a binary reaction. It is assumed that in our calculations, under naïve conditions only a proportion of outgrowth/branching is CRMP2-mediated. However, in CRMP2 overexpressing cells, a larger proportion of outgrowth/branching is attributable to CRMP2 and can, therefore, be targeted by LCM. It is unlikely that differences in IC_{50} values reflect separate actions of LCM. Whole-cell voltage clamp recordings from cortical neurons treated overnight with 30 μM LCM, a concentration higher than the IC_{50} for neurite inhibition in cells expressing endogenous levels of CRMP2, did not affect sodium currents or slow inactivation (*data not shown*). Voltage-gated calcium channels were also not affected by as much as 300 μM LCM (Wang and Khanna, 2011). These results suggest that subtherapeutic concentrations of LCM selectively block CRMP2-dependent neurite outgrowth without any effects on the sodium channels.

Mutation of the highest affinity lacosamide binding pocket on CRMP2 dramatically reduces LCM's effect on neurite complexity

In previous work using molecular modeling we identified cavities in the CRMP2 structure that could coordinate LCM binding (Wang et al., 2010a). A quintuplicate CRMP2 mutant ($CRMP2_{5ALA}$), harboring alanine mutations within the highest affinity LCM-binding pocket of CRMP2 (Figure 4A) was created using site-directed mutagenesis (Wang et al., 2010a). These mutations did not alter the protein's ability to mediate neurite dynamics, as the level of neurite complexity in the $CRMP2_{5ALA}$ mutant overexpressing neurons was not different from wildtype CRMP2-overexpressing neurons (Figure 4B). CRMP proteins have been shown to exist as heterotetramers (Wang and Strittmatter, 1997). Importantly, the ability to multimerize was not affected by these mutations (*data not shown*). Despite the enhanced neurite complexity seen following overexpression of the 5 alanine mutant, the IC_{50} value for inhibition of neurite complexity by LCM was calculated to be 25.7 ± 1.8 μM, almost exactly that of EGFP-overexpressing neurons (Figure 4C–D), suggesting that LCM is only targeting endogenous CRMP2. The inability of LCM to target $CRMP2_{5ALA}$- mediated enhancement

of outgrowth demonstrates that the effect is specific to LCM's interaction with CRMP2. To further verify the specificity of LCM's effect on neurite outgrowth, we repeated the aforementioned experiments following knockdown of endogenous CRMP2. Sholl analysis was performed 48 hours post-transfection with CRMP2 siRNA + GFP. As expected, the loss of CRMP2 expression (>90% loss of protein as assessed by immunoblot analyses (*data not shown*) reduced overall neurite outgrowth. Overnight application of 300 μM LCM did not lead to a further reduction in neurite complexity (Figure 5).

Lacosamide selectively impairs CRMP2-enhanced tubulin polymerization

The ability to bind and promote tubulin polymerization is necessary for CRMP2's role in neurite outgrowth and branching (Charrier et al., 2003). To investigate the mechanism behind the effect of LCM on CRMP2-mediated neurite dynamics, the amount of tubulin binding to CRMP2 was determined in the presence and absence of LCM. Co-immunoprecipitations were performed with a polyclonal CRMP2 antibody from postnatal day 1 rat brain lysates following 30 minute incubations in either DMSO or LCM. Co-immunoprecipitation of tubulin with CRMP2 was not altered by incubation of 3, 30, or 300 μM LCM (Figure 6A–B).

Distinct from its ability to bind tubulin, CRMP2 has been shown to accelerate tubulin polymerization by enhancing the GTPase activity of tubulin (Chae et al., 2009). To determine if this process was altered in the presence of LCM, microtubule polymerization was measured via a turbidimetric assay (Figure 6C). Purified tubulin and recombinant CRMP2 or $CRMP2_{5ALA}$ were combined in a glycerol-PEM buffer in the presence of DMSO or 3 μM LCM. Increases in tubulin polymerization were determined by measuring absorbance at 340nm every 30 seconds. To compare overall changes in tubulin polymerization, the area under the curve was calculated for each condition, using the first 5 measurements from the naïve condition (tubulin alone) as a baseline. Consistent with previous reports, addition of CRMP2 enhanced tubulin polymerization (Chae et al., 2009). Importantly, $CRMP2_{5ALA}$ also led to a similar enhancement. Co-application of 3 μM LCM prevented CRMP2- mediated enhancement of polymerization (Figure 6D). LCM failed to prevent $CRMP2_{5ALA}$-mediated enhancement of polymerization as the trending effect of LCM did not reach significance. In the absence of CRMP2 protein, tubulin polymerization was not altered by as much as 300 μM LCM (1.3 ± 0.5) versus naïve (0.4 ± 0.1; n=3, $p > 0.05$, Student's *t*-test) (*data not shown*). These results show that the effect of LCM is specific to CRMP2-mediated enhancement of tubulin polymerization.

Synaptic bouton size is not altered by LCM

As we have previously demonstrated that increased CRMP2 expression leads to an associated increase in synaptic bouton size (Brittain et al., 2009), the impact of LCM on this parameter was investigated (Figure 7A–B). The area of FM4-64 labeled presynaptic terminals in cortical neurons was determined following overnight incubation of 100 μM LCM, compared to 0.01% DMSO. Exposure to this level of LCM, sufficient enough to result in maximum reduction of CRMP2-mediated neurite outgrowth, did not alter bouton size. Consistent with these results, overnight exposure to LCM did not affect glutamate release from cortical neurons stimulated with high K^+ compared to 0.01% DMSO (Figure 7C–D). These results provide further evidence that LCM is selectively targeting the ability of CRMP2 to mediate neurite outgrowth.

Lacosamide prevents enhanced excitatory synaptic connectivity in an in vivo model of posttraumatic epileptogenesis

Axonal sprouting may play a critical role in epileptogenesis, particularly in posttraumatic and temporal lobe epilepsies (Nadler, 2003; Prince et al., 2009). In the partially isolated

cortex (undercut) model of posttraumatic epileptogenesis, axon sprouting has been demonstrated by morphological reconstruction of axons of the layer V pyramidal neurons (Salin et al., 1995) and by functional mapping of excitatory synaptic connectivity using laser scanning photostimulation of caged glutamate (Jin et al., 2006). To further test if LCM has the effect of preventing posttraumatic epileptogenesis and blocking axonal sprouting *in vivo*, we injected 100 mg/kg LCM for 7 days in rats that had received undercut surgery and used field potential recordings to monitor epileptiform activity and glutamate uncaging to map excitatory synaptic connectivity to cortical layer V pyramidal neurons (Figures 8–11).

In field potential recording experiments, there was no significant difference between the two groups in the percentage of animals exhibiting epileptiform activities. Epileptiform activities, including evoked and spontaneous interictal events, were recorded in slices from 4 of the 6 rats in the undercut (UC) group (67%) and from 4 of the 6 rats in the UC + LCM group (67%). However, the mean peak amplitude of the evoked epileptiform activities in the UC + LCM group was significantly lower than the UC group (Figure 8, 0.12 ± 0.03 mV in UC + saline group versus 0.05 ± 0.01 mV in UC + LCM group, $p<0.05$, Student's *t*-test).

In whole cell recordings, we first measured spontaneous excitatory postsynaptic currents (sEPSCs) at a holding potential of −70 mV. Administration of 100 mg/kg LCM caused a significant decrease in the frequency of sEPSCs, as indicated by the longer inter-event interval of sEPSCs (0.11 ± 0.01 s in the UC group versus 0.23 ± 0.05 s in the UC + LCM group, Figure 9B–C, $P<0.05$, student *t*-test), while no significant change in amplitudes was seen (Figure 9D, −9.9 ± 0.9 mV in the UC versus −11.5 ± 1.2 mV in the UC+LCM, $P>0.05$). The kinetics of the events were similar between the two groups, as indicated by lack of significant differences in 20–80% rise time, decay time constant, and half width of the events (*data not shown*). A decrease in the frequency of sEPSCs without change in event kinetics likely reflects a decrease in the number of synaptic contacts to these neurons. However, we can also not rule out the possibility that decreased probability of release may also contribute to this phenomenon.

For mapping excitatory synaptic connectivity, we first determined if there was any change in the responsiveness of cortical pyramidal neurons to glutamate uncaging by mapping evoked action potentials (APs). Most AP hotspots distributed within 150 μm of the somata (Figure 10). There was no significant difference between the UC and the UC+LCM treatment groups in the mean number of sites (hotspots) per map on which APs can be evoked (2.3 ± 0.32 in UC versus 2.0 ± 0.29 in UC+LCM group), AP spikes per map (4.9 ± 0.86 in UC versus 3.1 ± 0.82 in UC+LCM group), or AP spikes per hotspot (2.0 ± 0.2 in UC versus 1.4 ± 0.21 in UC + LCM) (Figure 10B, $p>0.05$ in all three comparisons).

Maps of excitatory synaptic connectivity expand in the undercut model of posttraumatic epileptogenesis (Jin et al., 2006). Following LCM treatment, we found that LCM treatment after injury caused a significant reduction in excitatory synaptic connectivity (Figure 11A–C). The mean hotspot ratio per map in the UC + LCM treatment group was much smaller than the UC group (0.51 ± 0.04 in UC versus 0.34 ± 0.02 in UC+LCM group, Figure 11D, E; $p<0.05$, student *t*-test). There was a trend of reduction in the normalized EPSC amplitude (−11.8 ± 3.1 mV in UC versus −5.0 ± 1.1 mV in UC+LCM group, $p=0.08$). Because there was no significant difference in the hotspot amplitude between the two groups (−20.1 ± 4.0 mV versus −14.3 ± 3.1 mV, $p>0.05$), the trend of reduction in normalized EPSC amplitude in UC+LCM group likely reflects a significant decrease in hotspot ratio.

Discussion

While the specific events following TBI which contribute to the development of posttraumatic epilepsy remain poorly understood, it is likely a combination of factors including disinhibition, increased excitability, and increased excitatory synaptic coupling (Graber and Prince, 2004; Prince et al., 2009). Robust axon sprouting and elongation occurs following in vitro lesion of axon collaterals and is sufficient to induce hyperexcitability and increased polysynaptic, epileptiform burst discharges (McKinney et al., 1997). Therefore, the increased excitatory connectivity following TBI may be a direct result of aberrant axon sprouting. The ability of lacosamide to target CRMP2, as well as, dampen excitability may place it at the forefront for the prevention of PTE.

A dual-mode of action has previously been proposed for LCM via its interactions with the voltage-gated sodium channel and CRMP2 (Beyreuther et al., 2007; Doty et al., 2007; Errington et al., 2008). Here we show that the interaction between LCM and CRMP2 has a functional impact on CRMP2, the presumed non-pharmacological target of LCM's action. The data demonstrate that LCM reduces CRMP2-mediated neurite complexity by impairing the ability of CRMP2 to enhance tubulin polymerization. Importantly, in vivo lacosamide treatment attenuated the increased excitatory connectivity associated with posttraumatic epilepsy.

LCM blocks CRMP2-mediated neurite complexity in vitro

Given the roles of CRMP2 in axonal elongation, neuronal differentiation, and polarity (Schmidt and Strittmatter, 2007), it is not surprising that CRMP2 may be linked to the aberrant axonal sprouting and subsequent increases in recurrent excitatory coupling in posttraumatic epilepsy. Therefore, it was important to determine the effects LCM may have on these growth parameters. Overexpression of CRMP2 led to increases in neurite branching which were attenuated by application of LCM at levels below those required for effective enhancement of sodium channel slow inactivation (Errington et al., 2008; Sheets et al., 2008). LCM is also able to alter the function of endogenous CRMP2, as the neurite complexity of EGFP-overexpressing neurons was decreased by LCM, though at higher concentrations than those over-expressing CRMP2. These differences in potency likely reflect the ability of LCM to target a larger percentage of the output measure (neurite outgrowth) under conditions of CRMP2-overexpression. As the level of CRMP2 expression is increased, so will the proportion of outgrowth attributable to CRMP2-function. That these morphological reductions were observed at concentrations of LCM lower than those reported as the clinical therapeutic plasma concentrations ((40–80 μM) (Greenaway et al., 2010)) compared to IC_{50} values obtained from these experiments: 3.5 ± 1.7 μM and 25.7 ± 1.9 μM for CRMP2-EGFP and EGFP-overexpressing neurons, respectively) further supports our hypothesis that LCM's mode of action involves CRMP2 in addition to its action on Na^+ channels.

LCM-induced reduction in neurite complexity is specific to CRMP2

Application of other sodium channel modulators did not affect neurite outgrowth, suggesting that the reduction in neurite complexity is independent of LCM's effect on voltage-gated sodium channels. Mutations within the primary binding pocket for LCM on CRMP2 returned the IC_{50} for inhibition of CRMP2-mediated enhancement of neurite complexity to levels identical to EGFP-overexpressing neurons. This finding suggests that, despite the presence of enhanced neurite complexity similar to wildtype CRMP2-overexpressing cells, LCM is only affecting endogenous CRMP2 in this system.

How does LCM mediate the inhibitory effects on CRMP2?

CRMP2 mediates neurite dynamics via regulation of microtubule assembly through two distinct mechanisms. CRMP2 binds and transports tubulin dimers to the distal end of the microtubule to promote polymerization (Gu and Ihara, 2000; Fukata et al., 2002; Kimura et al., 2005). Binding of tubulin to CRMP2 was not altered by LCM, even at concentrations 10-fold higher than the IC_{50} for reduction in neurite complexity. Nevertheless, given that CRMPs exist as heterotetramers (Wang and Strittmatter, 1997; Schmidt and Strittmatter, 2007), LCM's effects on CRMPs may also be dependent on the subunit composition of the tetramer.

CRMP2 can also promote microtubule assembly by enhancing the GTPase activity of tubulin (Chae et al., 2009). The presence of CRMP2 protein produced a marked increase in the rate and extent of tubulin polymerization. This increase in polymerization was reduced by application of LCM. Importantly, LCM did not alter basal levels of tubulin polymerization (i.e., in the absence of CRMP2), suggesting that LCM impairs the ability of CRMP2 to enhance tubulin's GTPase activity. Addition of the CRMP2 mutant ($CRMP2_{5ALA}$) enhanced tubulin polymerization similar to wildtype, yet was only marginally impaired by the application of LCM. The trending effect of LCM on $CRMP2_{5ALA}$ can be attributed to partial binding to the four additional binding pockets that were previously identified (Wang et al., 2010a). Additionally, the region on CRMP2 responsible for enhancing GTPase activity of tubulin lies within residues 480–509 (Chae et al., 2009). Since the binding pockets for LCM are in proximity to this domain (i.e. prime binding pocket residues: E360, S363, K418, I420, and P443), it is possible that the binding of LCM may decrease CRMP2-enhanced microtubule assembly by altering the accessibility of the GTPase accelerating domain of CRMP2 to its effectors. These results demonstrate that the decrease in CRMP2-mediated neurite dynamics by LCM is likely attributed to LCM's effect on CRMP2-enhanced tubulin polymerization.

Lacosamide attenuates axon sprouting and excitatory synaptic connectivity in vivo

Laser scanning photostimulation with caged glutamate has been used as an efficient technique for mapping synaptic circuitry under normal and pathological conditions (Callaway and Katz, 1993, Schubert et al., 2001, Jin et al., 2006, Bureau et al., 2008). Such monosynaptic functional maps are dependent on and reveal changes in pattern and strength of anatomical connections, such as axon sprouting in models of acquired epilepsies (Shepherd et al., 2003, Jin et al., 2006, Zhang et al., 2012). Using this technique, we further demonstrated that *in vivo* administration of LCM significantly reduced the hotspot ratio, but not amplitude, in maps of excitatory monosynaptic connectivity. These changes indicate that: (1) fewer cortical neurons maintain excitatory synaptic connection with layer V pyramidal neurons and (2) the strength of synaptic connections from neurons within each hotspot to the recorded neurons does not alter significantly.

A reduction in synaptic connectivity can result from reduced excitability of presynaptic neurons, reduced efficacy of synaptic transmission, or reduced anatomical synaptic connections between pre- and postsynaptic neurons. No significant change in neuronal excitability was detected under the existing conditions of photostimulation (Figure 8). Lack of significant differences in the kinetics and amplitude of sEPSCs (Figure 11) and in uncaging-evoked hotspot amplitudes suggest that LCM treatment did not reduce the efficacy of excitatory synaptic transmission. A decrease in the frequency of the sEPSCs without a change in the amplitude may result from a decrease in network excitability, a lower release probability of neurotransmitter, or fewer presynaptic terminals. Because our slice experiments were made one week after the end of LCM treatment and LCM only inhibits sustained repetitive firing (10 seconds duration) but not within the first second (Errington et

al., 2008), it is unlikely that LCM would directly induce substantial changes in network activity in our recording conditions and contribute to the deceased frequency of EPSCs. On the other hand, increased probability of release from excitatory presynaptic terminals has been demonstrated in neurons in this model of post-traumatic epileptogenesis (Li and Prince 2005). Our results in neuronal culture suggest that LCM does not directly affect glutamate release (Figure 7C, D), but the possibility that chronic LCM treatment may affect release probability still cannot be ruled out and requires further study. Nevertheless, the decrease in sEPSC frequency is consistent with a significant reduction in map size, and supports the notion that layer V pyramidal neurons receive less synaptic input. While direct morphological analysis was not obtained from layer V neurons, functional evidence together with data from *in vitro* experiments (Figures 2–5) suggests that LCM-induced reduction in excitatory synaptic connectivity is likely due to a blockade of axon sprouting.

Increased sprouting in the neocortical isolation model of PTE is associated with the formation of excessive excitatory circuits (Jin et al., 2006). However, the fundamental role of this process in epileptogenesis is unclear. It is likely that increased connectivity, in combination with increased excitability and decreased inhibition, directly contributes to the development of spontaneous seizure activity (Graber and Prince, 2004; Prince et al., 2009). The only successful attempt to prevent epileptogenesis in this model involved implantation of a tetrodotoxin (TTX)-infused polymer directly upon the isolated cortical regions (Graber and Prince, 1999). Importantly, application of TTX at later time points did not prevent epileptogenesis despite identical block of sodium channels. As TTX is capable of inducing complete synaptic blockade (Chiaia et al., 1994), an activity-dependent mechanism during a critical period may underlie epileptogenesis in this model (Graber and Prince, 2004). Interestingly, work in organotypic slice culture has demonstrated activity-dependent increases in axonal sprouting (Chen et al., 2005). While the anti-epileptogenic properties of TTX in this model may be due to complete synaptic blockade, the effect on axonal sprouting and excitatory connectivity has unfortunately not been established.

In vivo administration of LCM did not significantly reduce the occurrence of epileptiform activities in the undercut model. Possible explanations for the ineffectiveness of LCM may include inappropriate LCM treatment regimen (we injected a single dose of LCM for a period of seven days), insufficiency of blocking axon sprouting alone for preventing posttraumatic epileptogenesis, and/or compensatory reactions caused by LCM that would promote hyperexcitability through other mechanisms. However, the observed reduction in the amplitude of epileptiform activities is consistent with the reduced excitatory connectivity and may contribute to an anti-epileptogenic effect. In models of temporal lobe epilepsy, controversial results have been reported on the effects of inhibiting axonal sprouting on epileptogenesis. For example, successful prevention of mossy fiber sprouting by mTOR inhibition reduces spontaneous seizure frequency in kainate- (Zeng et al., 2009) but not pilocarpine-induced temporal lobe epilepsy (Buckmaster and Lew, 2011). Thus, the mechanisms contributing to epileptogenesis may differ depending on the model employed. Indeed, hypothermia has been shown to prevent mossy fiber sprouting and subsequently reduce seizure susceptibility following moderate TBI (Atkins et al., 2010). Interestingly, the presence of recurrent mossy fiber projections directly correlates with a transient decrease in the expression of the chemorepellant semaphorin3A, a negative regulator of CRMP2 function (Holtmaat et al., 2003). Given the prevalence of axonal sprouting following injury, as well as the potential involvement of semaphorin signaling, CRMP2-mediated axonal sprouting in response to TBI remains a valid target for the prevention of posttraumatic epileptogenesis.

In conclusion, this study has shown that the interaction of LCM with CRMP2 may have a disease modifying effect. LCM, at concentrations below that needed for its effects on Na^+

channels, blocks neurite outgrowth and complexity. Our data suggest that LCM administration reduces excitatory synaptic connectivity to layer V pyramidal neurons by inhibiting posttraumatic axon sprouting. Inhibition of CRMP2–mediated axonal growth and dendritic complexity by LCM may have important implications for synaptic reorganization, growth, and plasticity in epilepsy as well as in other pathophysiological conditions. It would be interesting to further determine if LCM application would prevent epileptogenesis and if interfering with the CRMP2 pathway is a novel therapeutic target for the prevention of neocortical posttraumatic epileptogenesis. It has become increasingly clear, as attempts to prevent PTE have proven unsuccessful, that the approaches for the treatment and prevention of PTE may not converge. The ability of lacosamide to target not only activity but CRMP2-mediated synaptic reorganization as well may afford efficacy in the prevention of posttraumatic epilepsy where so many classical antiepileptics have failed.

- Lacosamide targets Na^+ channels and collapsin response mediator protein 2 (CRMP2)
- Lacosamide inhibits CRMP2-mediated neurite outgrowth and tubulin polymerization
- CRMP2 mutant with reduced lacosamide binding has blunted neurite inhibitory effect
- Lacosamide prevents enhanced excitatory synaptic connectivity *in vivo*
- Lacosamide interacts with CRMP2 to inhibit posttraumatic axon sprouting

Acknowledgments

We thank members of the SNRI for discussions, Dr. May Khanna (IUSM) for help with Pymol figures, Stephanie Martinez for acquiring some of the confocal images, and Nicole Ashpole for providing some of the cortical neurons. S.M.W. is a Stark Scholar. J.D.H. is supported by an undergraduate Life-Health Sciences Internship. J.M.B. is supported by a Larry Kays Fellowship. This project was supported by a Project Development Team within the ICTSI NIH/NCRR Grant Number RR025761 (A70-9-079138 to R.K.), NIH grant NS057940 (to X.J.) and the Elwert Award in Medicine (to R.K. and to X.J.).

Abbreviations

AED	antiepileptic drug
AP	action potential
CRMP2	collapsin response mediator protein
DIV	days in vitro
EGFP	enhanced green fluorescent protein
LCM	(R)-*N*-benzyl 2-acetomido-3-methoxypropionamide
MPL	N-Methylpyrrolidone
PTE	posttraumatic epilepsy
sEPSCs	spontaneous excitatory postsynaptic currents
siRNA	short interfering RNA
TBI	traumatic brain injury
UC	undercut model

VGSCs voltage-gated sodium channels

References

Atkins CM, Truettner JS, Lotocki G, Sanchez-Molano J, Kang Y, Alonso OF, Sick TJ, Dietrich WD, Bramlett HM. Post-traumatic seizure susceptibility is attenuated by hypothermia therapy. Eur J Neurosci. 2010; 32:1912–1920. [PubMed: 21044182]

Beyreuther BK, Freitag J, Heers C, Krebsfanger N, Scharfenecker U, Stohr T. Lacosamide: a review of preclinical properties. CNS Drug Rev. 2007; 13:21–42. [PubMed: 17461888]

Brittain JM, Chen L, Wilson SM, Brustovetsky T, Gao X, Ashpole NM, Molosh AI, You H, Hudmon A, Shekhar A, White FA, Zamponi GW, Brustovetsky N, Chen J, Khanna R. (Neuroprotection against traumatic brain injury by a peptide derived from the collapsin response mediator protein 2 (CRMP2). J Biol Chem. 2011a; 286:37778–37792. [PubMed: 21832084]

Brittain JM, Duarte DB, Wilson SM, Zhu W, Ballard C, Johnson PL, Liu N, Xiong W, Ripsch MS, Wang Y, Fehrenbacher JC, Fitz SD, Khanna M, Park CK, Schmutzler BS, Cheon BM, Due MR, Brustovetsky T, Ashpole NM, Hudmon A, Meroueh SO, Hingtgen CM, Brustovetsky N, Ji RR, Hurley JH, Jin X, Shekhar A, Xu XM, Oxford GS, Vasko MR, White FA, Khanna R. Suppression of inflammatory and neuropathic pain by uncoupling CRMP-2 from the presynaptic Ca^{2+} channel complex. Nat Med. 2011b; 17:822–829. [PubMed: 21642979]

Brittain JM, Piekarz AD, Wang Y, Kondo T, Cummins TR, Khanna R. An atypical role for collapsin response mediator protein 2 (CRMP-2) in neurotransmitter release via interaction with presynaptic voltage-gated calcium channels. J Biol Chem. 2009; 284:31375–31390. [PubMed: 19755421]

Buckmaster PS, Lew FH. Rapamycin suppresses mossy fiber sprouting but not seizure frequency in a mouse model of temporal lobe epilepsy. J Neurosci. 2011; 31:2337–2347. [PubMed: 21307269]

Bureau I, Shepherd GM, Svoboda K. Circuit and plasticity defects in the developing somatosensory cortex of FMR1 knock-out mice. J Neurosci. 2008; 28:5178–5188. [PubMed: 18480274]

Callaway EM, Katz LC. Photostimulation using caged glutamate reveals functional circuitry in living brain slices. Proc Natl Acad Sci U S A. 1993; 90:7661–7665. [PubMed: 7689225]

Carlier MF, Pantaloni D. Taxol effect on tubulin polymerization and associated guanosine 5'-triphosphate hydrolysis. Biochemistry (Mosc). 1983; 22:4814–4822.

Chae YC, Lee S, Heo K, Ha SH, Jung Y, Kim JH, Ihara Y, Suh PG, Ryu SH. Collapsin response mediator protein-2 regulates neurite formation by modulating tubulin GTPase activity. Cell Signal. 2009; 21:1818–1826. [PubMed: 19666111]

Charrier E, Reibel S, Rogemond V, Aguera M, Thomasset N, Honnorat J. Collapsin response mediator proteins (CRMPs): involvement in nervous system development and adult neurodegenerative disorders. Mol Neurobiol. 2003; 28:51–64. [PubMed: 14514985]

Chen S, Hirata K, Ren Y, Sugimori M, Llinas R, Hillman DE. Robust axonal sprouting and synaptogenesis in organotypic slice cultures of rat cerebellum exposed to increased potassium chloride. Brain Res. 2005; 1057:88–97. [PubMed: 16125152]

Chi XX, Schmutzler BS, Brittain JM, Wang Y, Hingtgen CM, Nicol GD, Khanna R. Regulation of N-type voltage-gated calcium channels (Cav2.2) and transmitter release by collapsin response mediator protein-2 (CRMP-2) in sensory neurons. J Cell Sci. 2009; 122:4351–4362. [PubMed: 19903690]

Chiaia NL, Fish SE, Bauer WR, Figley BA, Eck M, nett-Clarke CA, Rhoades RW. Effects of postnatal blockage of cortical activity with tetrodotoxin upon lesion-induced reorganization of vibrissae-related patterns in the somatosensory cortex of rat. Brain Res Dev Brain Res. 1994; 79:301–306.

Choi D, Stables JP, Kohn H. The anticonvulsant activities of functionalized N-benzyl 2-acetamidoacetamides. The importance of the 2-acetamido substituent. Bioorg Med Chem. 1996; 4:2105–2114. [PubMed: 9022975]

Curia G, Biagini G, Perucca E, Avoli M. Lacosamide: a new approach to target voltage-gated sodium currents in epileptic disorders. CNS Drugs. 2009; 23:555–568. [PubMed: 19552484]

Diaz-Arrastia R, Agostini MA, Madden CJ, Van Ness PC. Posttraumatic epilepsy: The endophenotypes of a human model of epileptogenesis. Epilepsia. 2009; 50:14–20. [PubMed: 19187290]

Doty P, Rudd GD, Stoehr T, Thomas D. Lacosamide. Neurotherapeutics. 2007; 4:145–148. [PubMed: 17199030]

Errington AC, Coyne L, Stohr T, Selve N, Lees G. Seeking a mechanism of action for the novel anticonvulsant lacosamide. Neuropharmacology. 2006; 50:1016–1029. [PubMed: 16620882]

Errington AC, Stohr T, Heers C, Lees G. The investigational anticonvulsant lacosamide selectively enhances slow inactivation of voltage-gated sodium channels. Mol Pharmacol. 2008; 73:157–169. [PubMed: 17940193]

Fukata Y, Itoh TJ, Kimura T, Menager C, Nishimura T, Shiromizu T, Watanabe H, Inagaki N, Iwamatsu A, Hotani H, Kaibuchi K. CRMP-2 binds to tubulin heterodimers to promote microtubule assembly. Nat Cell Biol. 2002; 4:583–591. [PubMed: 12134159]

Golarai G, Greenwood AC, Feeney DM, Connor JA. Physiological and structural evidence for hippocampal involvement in persistent seizure susceptibility after traumatic brain injury. J Neurosci. 2001; 21:8523–8537. [PubMed: 11606641]

Graber KD, Prince DA. Tetrodotoxin prevents posttraumatic epileptogenesis in rats. Ann Neurol. 1999; 46:234–242. [PubMed: 10443889]

Graber KD, Prince DA. A critical period for prevention of posttraumatic neocortical hyperexcitability in rats. Ann Neurol. 2004; 55:860–870. [PubMed: 15174021]

Granacher, R. Traumatic Brain Injury: Methods for Clinical and Forensic Neuropsychiatric Assessment. Boca Raton, Fl: CRC Press LLC; 2003.

Greenaway C, Ratnaraj N, Sander JW, Patsalos PN. A high-performance liquid chromatography assay to monitor the new antiepileptic drug lacosamide in patients with epilepsy. Ther Drug Monit. 2010; 32:448–452. [PubMed: 20386357]

Gu Y, Ihara Y. Evidence that collapsin response mediator protein-2 is involved in the dynamics of microtubules. J Biol Chem. 2000; 275:17917–17920. [PubMed: 10770920]

Harris JA, Murphy JA. Lacosamide: an adjunctive agent for partial-onset seizures and potential therapy for neuropathic pain. Ann Pharmacother. 2009; 43:1809–1817. [PubMed: 19843834]

Hoffman SN, Salin PA, Prince DA. Chronic neocortical epileptogenesis in vitro. J Neurophysiol. 1994; 71:1762–1773. [PubMed: 8064347]

Holtmaat AJGD, Gorter JA, Wit JD, Tolner EA, Spijker S, Giger RJ, Lopes da Silva FH, Verhaagen J. Transient downregulation of sema3a mrna in a rat model for temporal lobe epilepsy: A novel molecular event potentially contributing to mossy fiber sprouting. Exp Neurol. 2003; 182:142–150. [PubMed: 12821384]

Inagaki N, Chihara K, Arimura N, Menager C, Kawano Y, Matsuo N, Nishimura T, Amano M, Kaibuchi K. CRMP-2 induces axons in cultured hippocampal neurons. Nat Neurosci. 2001; 4:781–782. [PubMed: 11477421]

Jin X, Huguenard JR, Prince DA. Reorganization of inhibitory synaptic circuits in rodent chronically injured epileptogenic neocortex. Cereb Cortex. 2011; 21:1094–1104. [PubMed: 20855494]

Jin X, Prince DA, Huguenard JR. Enhanced excitatory synaptic connectivity in layer v pyramidal neurons of chronically injured epileptogenic neocortex in rats. J Neurosci. 2006; 26:4891–4900. [PubMed: 16672663]

Kelemen A, Halasz P. Lacosamide for the prevention of partial onset seizures in epileptic adults. Neuropsychiatr Dis Treat. 2010; 6:465–471. [PubMed: 20856610]

Kharatishvili I, Nissinen JP, McIntosh TK, Pitkänen A. A model of posttraumatic epilepsy induced by lateral fluid-percussion brain injury in rats. Neuroscience. 2006; 140:685–697. [PubMed: 16650603]

Kimura T, Watanabe H, Iwamatsu A, Kaibuchi K. Tubulin and CRMP-2 complex is transported via Kinesin-1. J Neurochem. 2005; 93:1371–1382. [PubMed: 15935053]

Lees G, Stöhr T, Errington AC. Stereoselective effects of the novel anticonvulsant lacosamide against 4-AP induced epileptiform activity in rat visual cortex in vitro. Neuropharmacology. 2006; 50:98–110. [PubMed: 16225894]

McKinney RA, Debanne D, Gahwiler BH, Thompson SM. Lesion-induced axonal sprouting and hyperexcitability in the hippocampus in vitro: implications for the genesis of posttraumatic epilepsy. Nat Med. 1997; 3:990–996. [PubMed: 9288725]

Nadler JV. The Recurrent Mossy Fiber Pathway of the Epileptic Brain. Neurochem Res. 2003; 28:1649–1658. [PubMed: 14584819]

Nishimura T, Fukata Y, Kato K, Yamaguchi T, Matsuura Y, Kamiguchi H, Kaibuchi K. CRMP-2 regulates polarized Numb-mediated endocytosis for axon growth. Nat Cell Biol. 2003; 5:819–826. [PubMed: 12942088]

Park KD, Morieux P, Salome C, Cotten SW, Reamtong O, Eyers C, Gaskell SJ, Stables JP, Liu R, Kohn H. Lacosamide isothiocyanate-based agents: novel agents to target and identify lacosamide receptors. J Med Chem. 2009; 52:6897–6911. [PubMed: 19795888]

Perucca E, Yasothan U, Clincke G, Kirkpatrick P. Lacosamide. Nat Rev Drug Discov. 2008; 7:973–974. [PubMed: 19043448]

Prince DA, Parada I, Scalise K, Graber K, Jin X, Shen F. Epilepsy following cortical injury: Cellular and molecular mechanisms as targets for potential prophylaxis. Epilepsia. 2009; 50:30–40. [PubMed: 19187292]

Salin P, Tseng GF, Hoffman S, Parada I, Prince DA. Axonal sprouting in layer V pyramidal neurons of chronically injured cerebral cortex. J Neurosci. 1995; 15:8234–8245. [PubMed: 8613757]

Schmidt EF, Strittmatter SM. The CRMP family of proteins and their role in Sema3A signaling. Adv Exp Med Biol. 2007; 600:1–11. [PubMed: 17607942]

Schubert D, Staiger JF, Cho N, Kotter R, Zilles K, Luhmann HJ. Layer-specific intracolumnar and transcolumnar functional connectivity of layer V pyramidal cells in rat barrel cortex. J Neurosci. 2001; 21:3580–3592. [PubMed: 11331387]

Sheets PL, Heers C, Stoehr T, Cummins TR. Differential block of sensory neuronal voltage-gated sodium channels by lacosamide [(2R)-2-(acetylamino)-N-benzyl-3-methoxypropanamide], lidocaine, and carbamazepine. J Pharmacol Exp Ther. 2008; 326:89–99. [PubMed: 18378801]

Shepherd GM, Pologruto TA, Svoboda K. Circuit analysis of experience-dependent plasticity in the developing rat barrel cortex. Neuron. 2003; 38:277–289. [PubMed: 12718861]

Sholl DA. Dendritic organization in the neurons of the visual and motor cortices of the cat. J Anat. 1953; 87:387–406. [PubMed: 13117757]

Temkin NR. Preventing and treating posttraumatic seizures: The human experience. Epilepsia. 2009; 50:10–13. [PubMed: 19187289]

Wang LH, Strittmatter SM. A family of rat CRMP genes is differentially expressed in the nervous system. J Neurosci. 1996; 16:6197–6207. [PubMed: 8815901]

Wang LH, Strittmatter SM. Brain CRMP forms heterotetramers similar to liver dihydropyrimidinase. J Neurochem. 1997; 69:2261–2269. [PubMed: 9375656]

Wang Y, Brittain JM, Jarecki BW, Park KD, Wilson SM, Wang B, Hale R, Meroueh SO, Cummins TR, Khanna R. In silico docking and electrophysiological characterization of lacosamide binding sites on collapsin response mediator protein 2 (CRMP-2) identifies a pocket important in modulating sodium channel slow inactivation. J Biol Chem. 2010a; 285:25296–25307. [PubMed: 20538611]

Wang Y, Brittain JM, Wilson SM, Hingtgen CM, Khanna R. Altered Calcium Currents and Axonal Growth in Nf1 Haploinsufficient Mice. Transl Neurosci. 2010b; 1:106–114. [PubMed: 21949590]

Wang Y, Khanna R. Calcium channels are not affected by the anti-epileptic drug lacosamide. Transl Neurosci. 2011; 2:13–22. [PubMed: 21949591]

Xiong W, Ping X, Gao J, Jin X. Preparing Undercut Model of Posttraumatic Epileptogenesis in Rodents. JoVE. 2011:e2840.

Zeng LH, Rensing NR, Wong M. The mammalian target of rapamycin signaling pathway mediates epileptogenesis in a model of temporal lobe epilepsy. J Neurosci. 2009; 29:6964–6972. [PubMed: 19474323]

Zhang W, Huguenard JR, Buckmaster PS. Increased Excitatory Synaptic Input to Granule Cells from Hilar and CA3 Regions in a Rat Model of Temporal Lobe Epilepsy. J Neurosci. 2012; 32:1183–1196. [PubMed: 22279204]

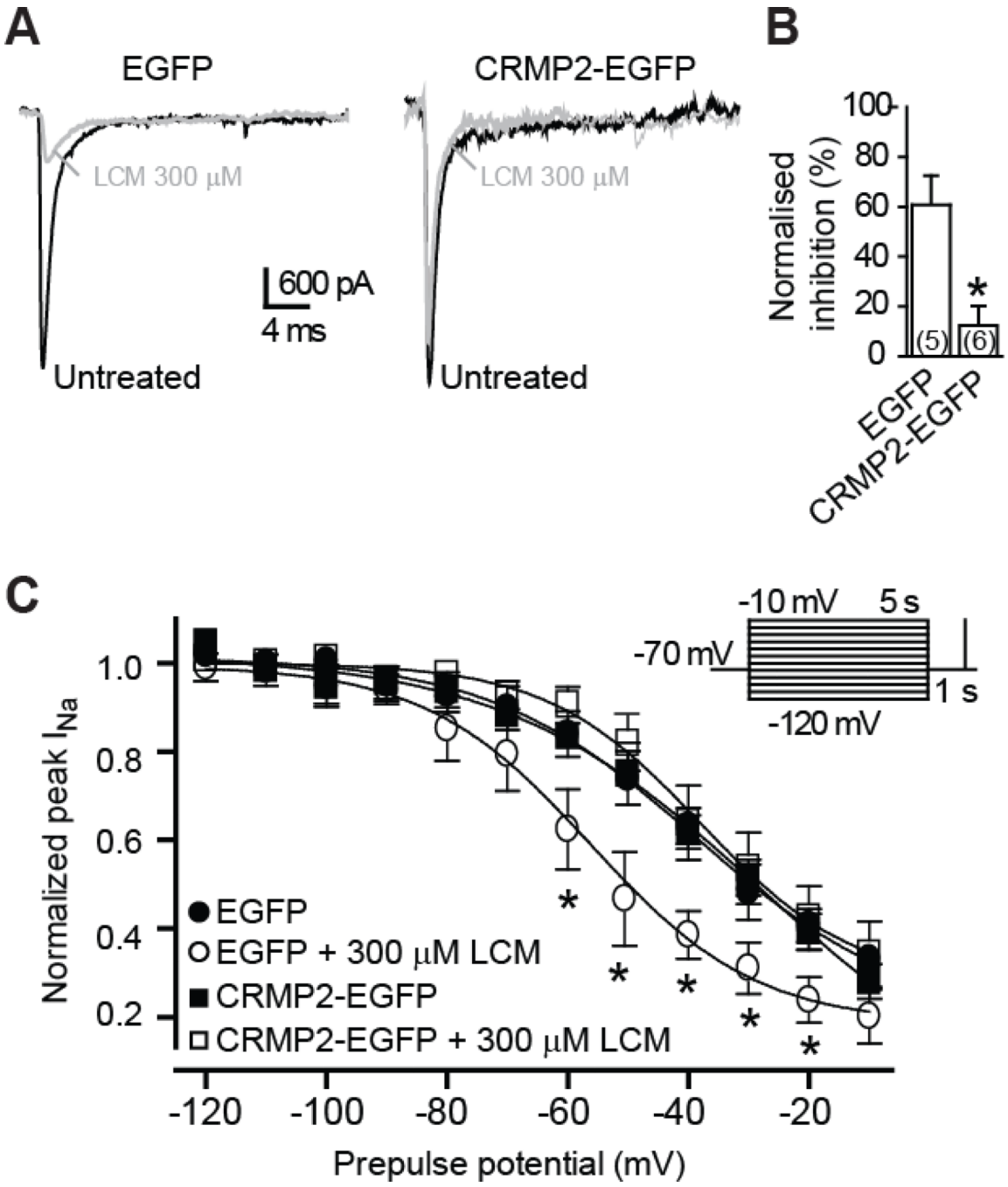

Figure 1. Over-expression of CRMP2 blunts effect of lacosamide on sodium channels

(**A**) Representative peak Na^+ currents, in response to a step to −10 mV from a holding potential of −100 mV, of neurons transfected with EGFP (*left*) or CRMP2-EGFP (*right*) in the absence (*black traces*) or presence of 300 μM LCM (*grey traces*). Peak currents were normalized to cell capacitance. (**B**) The maximal current evoked by a pulse to −10 mV was reduced significantly by LCM (*; $p < 0.05$, Student's *t*-test). Number in parentheses represents numbers of cells. (**C**) Inset: Voltage protocol for slow inactivation. Currents were evoked by 5 s prepulses between −120 mV and −10 mV and then fast inactivated channels were allowed to recover for 1 s at a hyperpolarized pulse to −70 mV. The fraction of

channels available at −10 mV was analyzed. Summary of steady-state slow activation curves for hippocampal neurons transfected with either EGFP or CRMP2–EGFP and incubated in control (0.01% MPL) or LCM (300 μM). CRMP2 over–expression blocked the development of LCM-induced slow inactivation which was observed in EGFP overexpressing neurons treated with LCM. In the presence of LCM, the midpoint (V_{50}) of slow inactivation in EGFP overexpressing neurons was shifted by almost 20 mV to more hyperpolarized potentials compared with untreated cells.

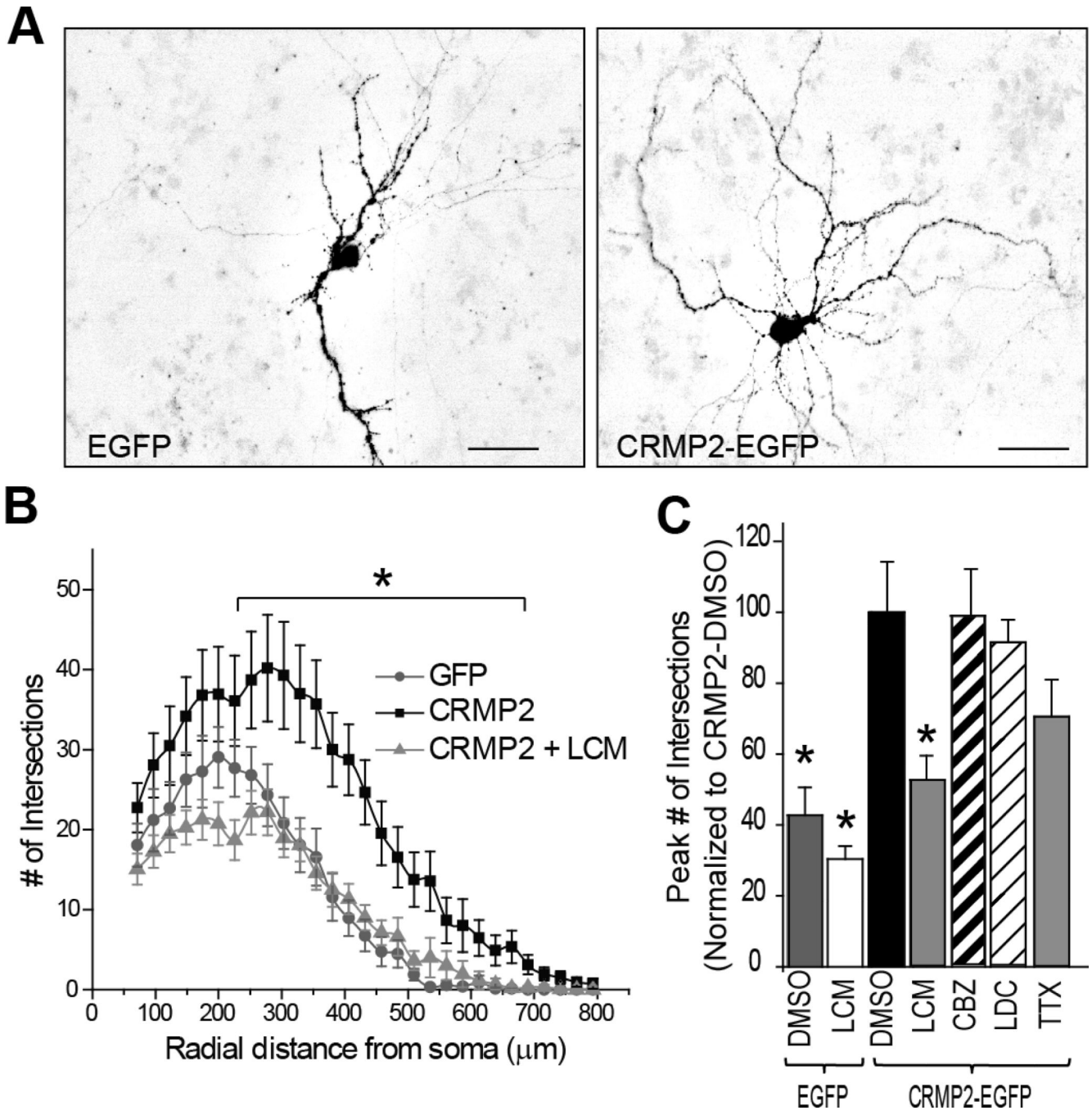

Figure 2. CRMP2-mediated enhancement in neurite complexity is blocked by the anticonvulsant lacosamide

(**A**) Representative inverted black and white images of cortical neurons 48 h after transfection with EGFP or CRMP2–EGFP. (**B**) Neuritic complexity was calculated by Sholl analysis of cultured cortical neurons transfected at 9 DIV (and grown for 48h). Peak numbers of intersections were observed at 275 μm from the soma. Significant increase in neuritic complexity was seen in CRMP2-EGFP neurons (*, $p < 0.05$ vs. EGFP at each distance between 250–700 μm; Student's *t*- test). Overnight application of 300 μM LCM in CRMP2-EGFP overexpressing neurons returned neuritic complexity to levels comparable to EGFP-overexpressing neurons. At least 17 neurons were analyzed, in a blinded manner for

each condition. (**C**) Summary of the average peak neuritic complexity for EGFP and CRMP2-EGFP transfected neurons treated with vehicle (0.01% DMSO), 300 μM LCM, 300 μM carbamezapine (CBZ), 200 μM lidocaine (LDC) or 100 nM tetrodotoxin (TTX). To allow direct comparison peak # of intersections are represented as a percentage of CRMP2-EGFP + DMSO. (n= 15–25 for each condition) (*, $p < 0.05$ versus CRMP2-DMSO; one-way ANOVA, Bonferroni's *post-hoc* analysis.)

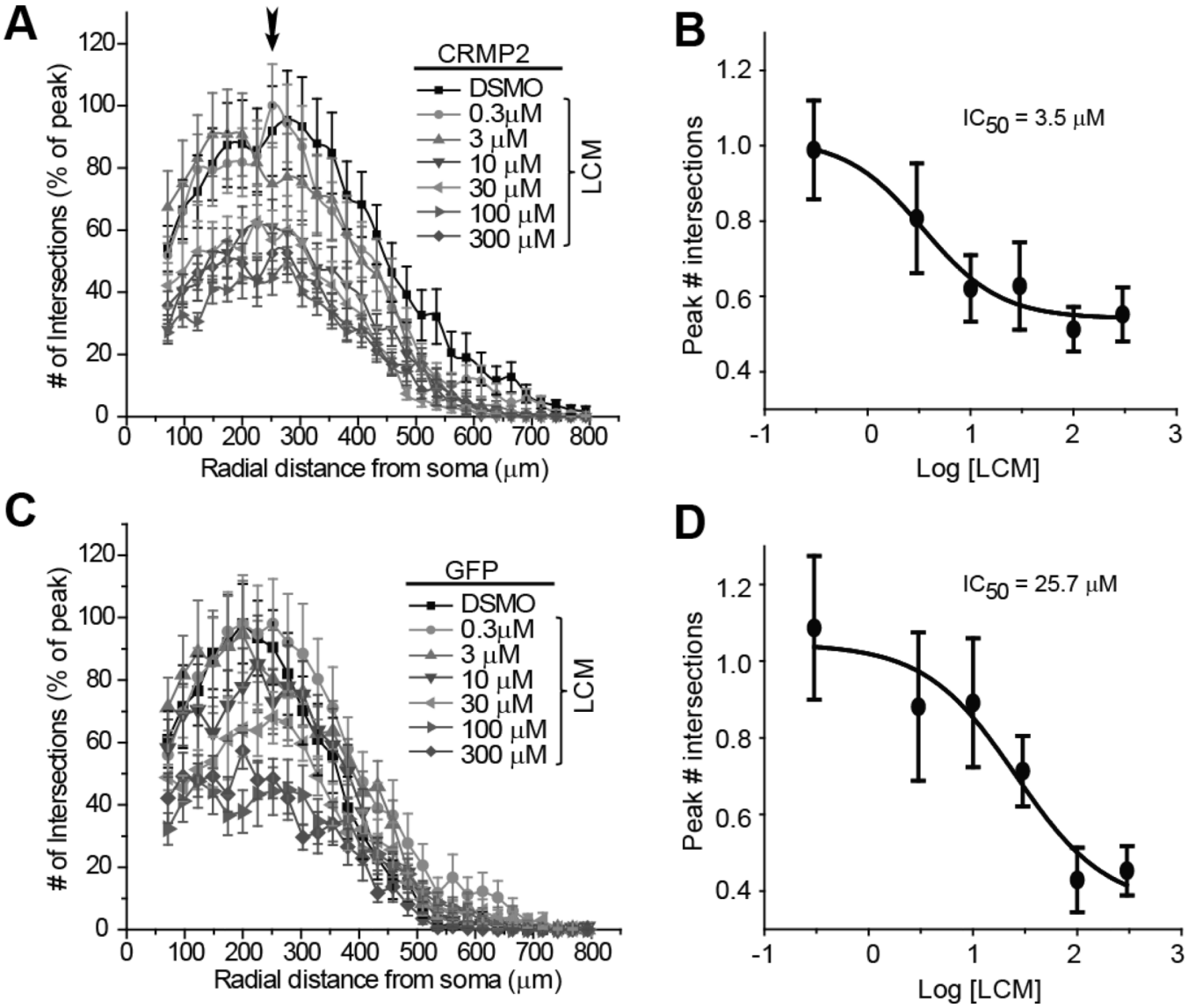

Figure 3. Lacosamide causes a dose-dependent reduction in neurite outgrowth of cortical neurons

Sholl analysis of cortical neurons transfected with CRMP2-EGFP (**A**) or EGFP (**C**) and treated for 24 hr with 0.3 μM to 300 μM LCM or 0.01% DMSO (control). To allow direct comparison of the effect of LCM between CRMP2-EGFP and EGFP expressing cells, number of intersections was normalized to the maximum number of intersections in each experiment. Arrow in **A** denotes the peak number of intersections, which occurred at ~275 μm radial distance from the soma. Logarithmic dose-response plots of mean peak # of intersections for CRMP2-EGFP (**B**) and EGFP (**D**) transfected neurons. Average peak # of intersections, obtained from the Sholl analyses, were normalized to the average peak # of intersections in the vehicle (DMSO)-treated condition. The IC_{50} for inhibition of neurite complexity by LCM was determined by fitting the curve to a Sigmoidal dose response function (n= 15–25 cells for each condition from at least 3 separate culture wells).

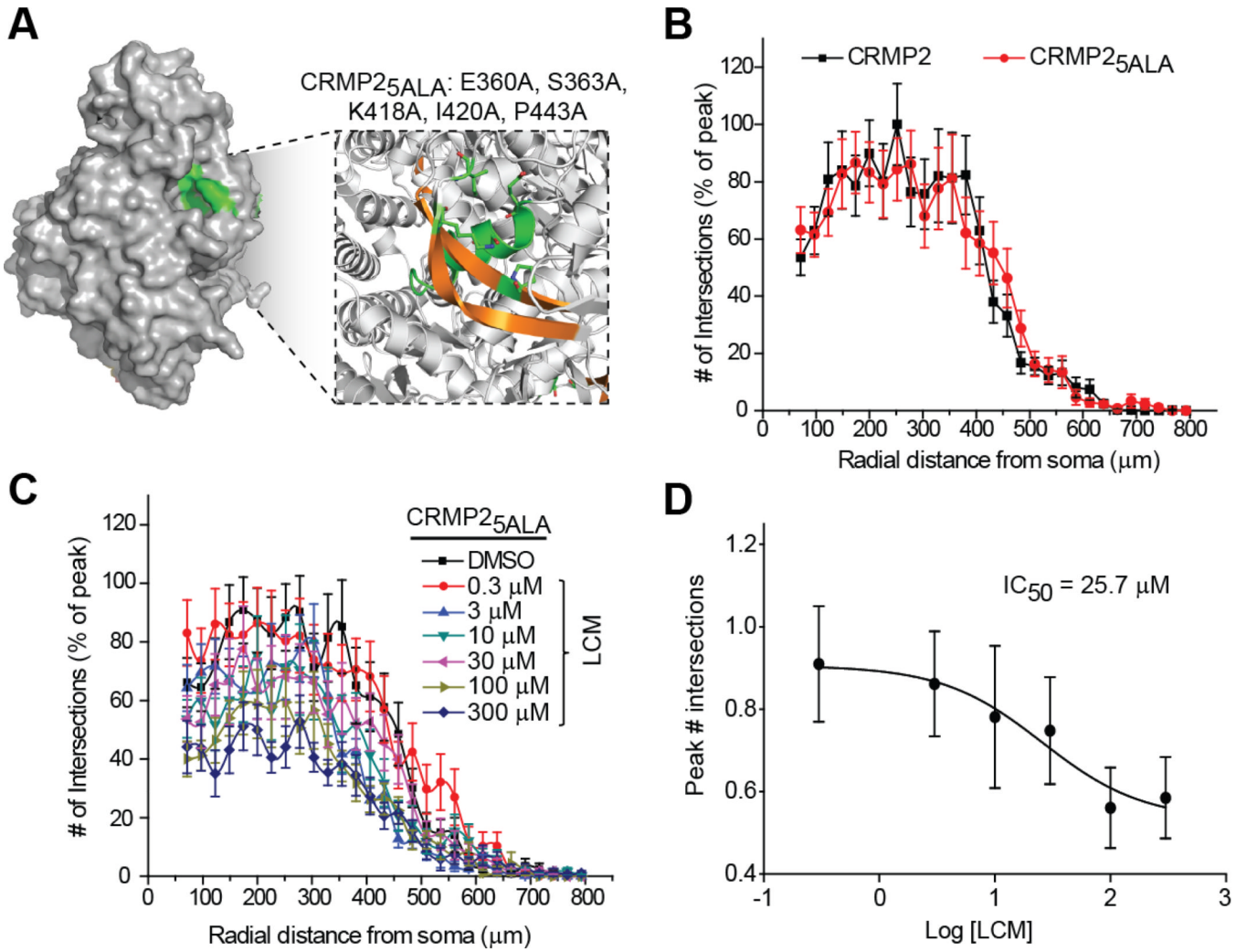

Figure 4. Mutating putative lacosamide coordinating sites within CRMP2 reduces lacosamide's inhibition of neurite outgrowth

(**A**) CRMP2 surface representation highlighting the location of the LCM-binding pocket (*green*). The box represents an enlarged view of the binding pocket highlighting the helices and beta-strands (*gold*) involved in coordinating LCM. The residues coordinating LCM are indicated in single amino acid letter code. (**B**) Sholl analyses of neurons expressing CRMP2 or CRMP2$_{5ALA}$. Mutation of the LCM coordinating residues does not impair the ability of this mutant protein to promote neurite complexity. (**C**) Sholl analyses of neurons expressing CRMP2$_{5ALA}$ and incubated in varying concentrations of LCM as indicated. (**D**) Logarithmic dose-response plot of mean peak # of intersections for CRMP2$_{5ALA}$ expressing neurons (n=15–25 cells per condition from at least 3 separate culture wells). The IC$_{50}$ for inhibition of neurite complexity by LCM was determined as described in the legend to Figure 2.

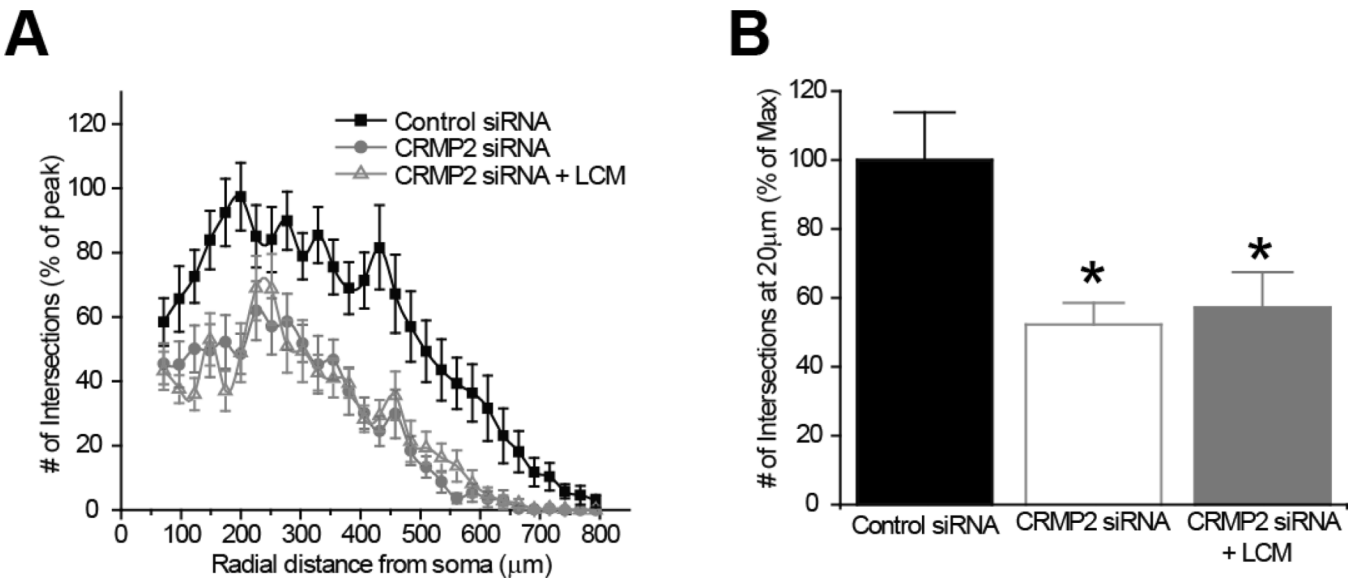

Figure 5. siRNA knockdown of CRMP2 reduces neurite outgrowth

(**A**) Sholl analysis of neurons transfected with control or CRMP2 siRNA ± 300μM LCM. (**B**) To allow direct comparisons, the number of intersections were compared at ~200 μm from the soma and expressed as a percentage of max. The siRNA knockdown of CRMP2 decreased neurite outgrowth (52.25 ± 6.24%) compared to control siRNA (100.02 ± 13.86%). Overnight incubation of 300 μM LCM did not cause a further decrease in complexity (57.13 ± 10.34%). (*, $p < 0.05$; One-Way ANOVA, Bonferroni *post-hoc* analysis).

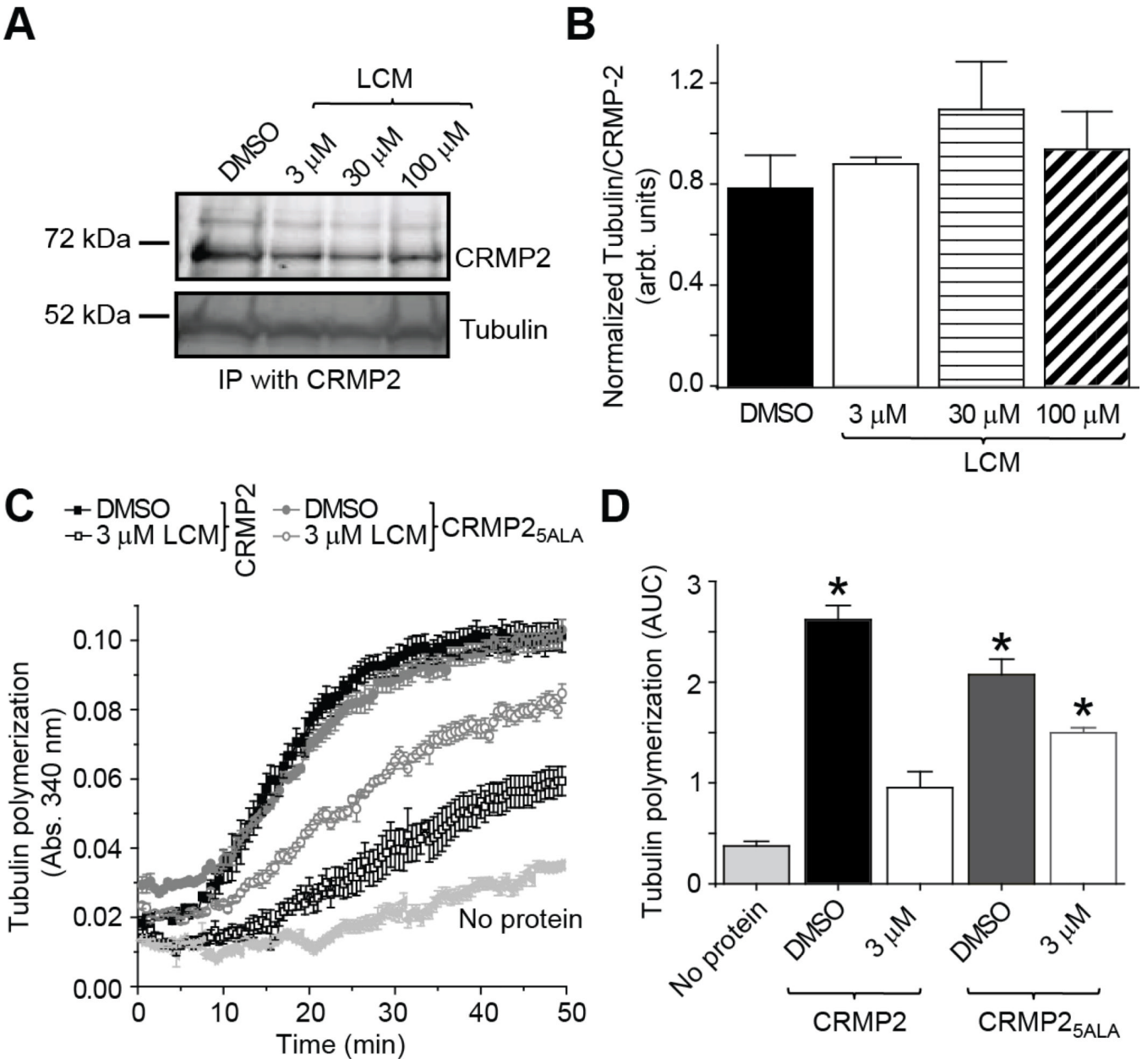

Figure 6. LCM reduces CRMP2-enhanced tubulin polymerization

(**A**) Co-immunoprecipitation of tubulin with CRMP2 in the presence of 3, 30 or 300 μM LCM compared to 0.01% DMSO (control). (**B**) LCM treatment did not affect the amount of tubulin co-immunoprecipitated with CRMP2 as determined by densitometric analysis (data represents arbitrary fluorescence units, n = 4). **(C**) Effects of CRMP2 and CRMP2$_{5ALA}$ recombinant proteins on microtubule assembly were measured by light scattering and absorbance at 340 nm. Similar levels of tubulin polymerization were facilitated by CRMP2 and CRMP2$_{5ALA}$ proteins. Inclusion of LCM (3 μM) with the CRMP2 protein caused a greater reduction in tubulin polymerization compared to a similar treatment of the CRMP2$_{5ALA}$ protein. Also shown is the basal tubulin self-polymerization in the absence of any protein (no protein). Values represent the means of three independent experiments. Background absorbance was subtracted from each experiment. (**D**) Average area under the curve (AUC) values ± SEM calculated from the tubulin polymerization curves shown in **A**.

Addition of 3 μM LCM led to a significant reduction in the tubulin polymerization AUC for wildtype CRMP2 (*, $p < 0.05$; One-Way ANOVA, Bonferroni *post-hoc* analysis). There was no statistical difference in the tubulin polymerization AUC for $CRMP2_{5ALA}$ in the absence or presence of LCM ($p > 0.05$, One-Way ANOVA, Bonferroni *post-hoc* analysis).

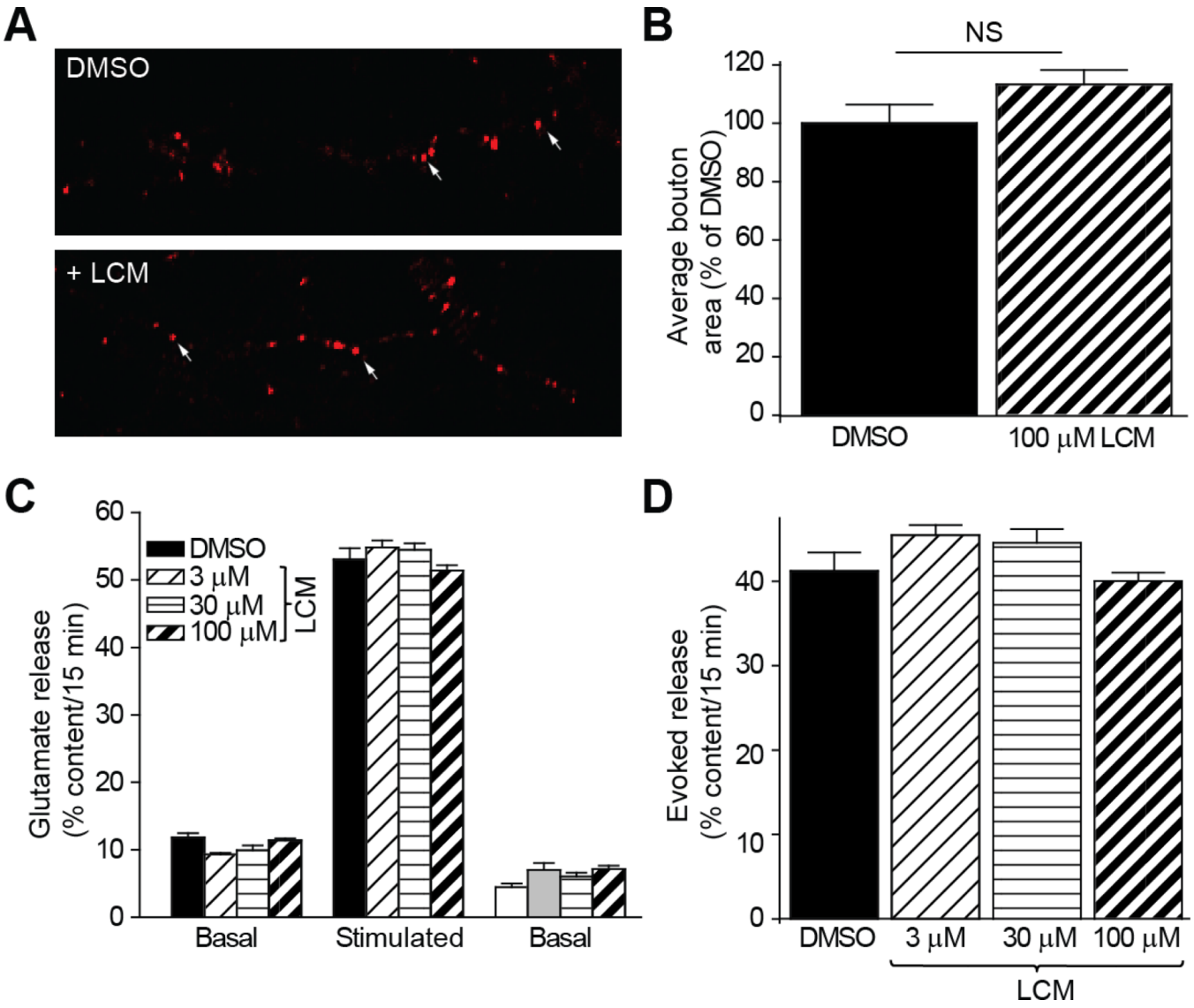

Figure 7. LCM does not alter synaptic bouton size or glutamate release

(**A**) FM4-64 loading of synaptic boutons in cortical neurons. Arrows denote representative boutons. (**B**) Overnight treatment with 100 μM LCM did not affect bouton area. The number of boutons counted ranged from 117 to 144. (**C**) Glutamate release from cortical neurons following overnight treatment with 3μM, 30μM, and 100μM LCM compared to 0.01% DMSO (control). Data are represented as percent of total glutamate content (n=6 wells per condition). (**D**) Evoked glutamate release following LCM treatment did not differ from control condition, where evoked release represents: (Stimulated-Basal) as a percent of total glutamate content.

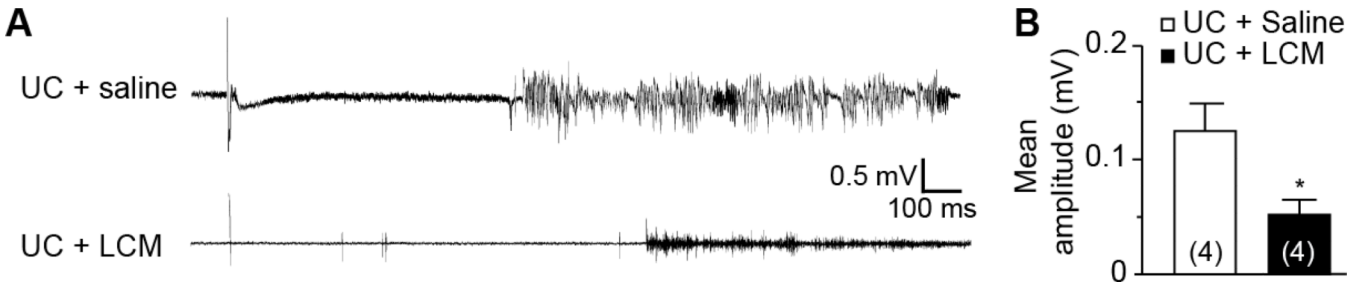

Figure 8. Effect of LCM treatment on epileptiform activities

(**A**) Exemplar traces showing evoked epileptiform events in the undercut rats without (top) and with (bottom) LCM treatment. (**B**) LCM treatment did not prevent the occurrence of epileptiform activities, but it caused a significant decrease in the mean amplitude of epileptiform activities in slices of the LCM treatment group ($P<0.05$, student *t*-test).

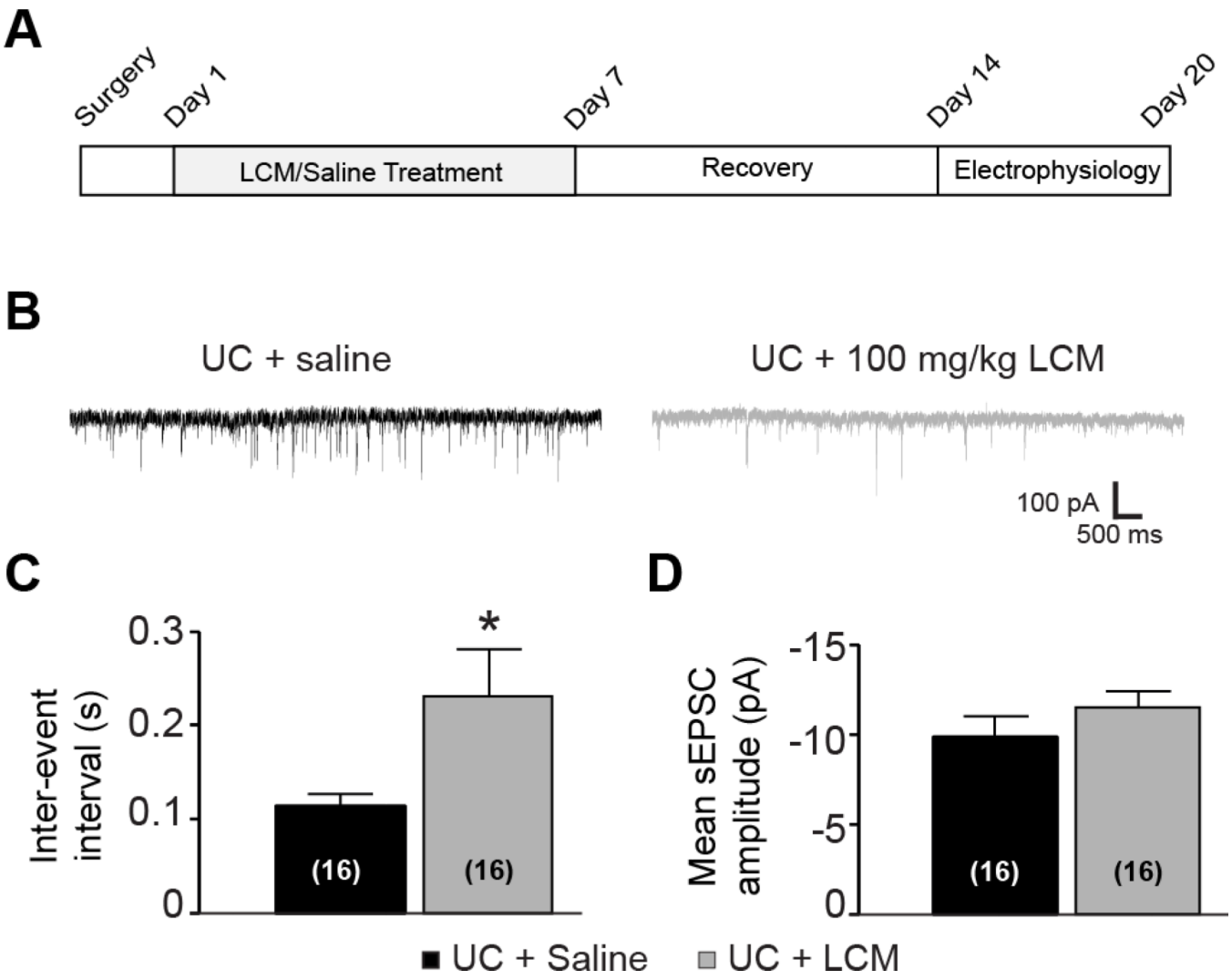

Figure 9. LCM decreases the frequency but not the amplitude of spontaneous EPSCs (sEPSCs) in posttraumatic cortical pyramidal neurons

(**A**) Timeline of experimental design. Undercut surgery is represented as day 0. LCM or saline treatment began 2 days following surgery and continued for 7 days. Animals were allowed to recover from treatment until neocortical slices were obtained, 14–20 days after surgery. (**B**) Representative evoked field potentials in cortical slices from areas of chronic undercut (UC) injury. Epileptiform activity was observed in 4/10 slices from UC animals receiving saline, compared to 1/9 slices from UC animals treated with LCM. (**C**) Representative traces of sEPSCs from cortical layer V pyramidal neurons in brain slices of undercut rats with saline (left) or 100 mg/kg LCM (right) treatments. (**D**) Mean inter-event interval of sEPSCs was significantly longer in the LCM treatment group than the control group ($P<0.05$, student *t*-test). (**D**) Mean amplitudes of sEPSCs were similar between the control and LCM treatment groups.

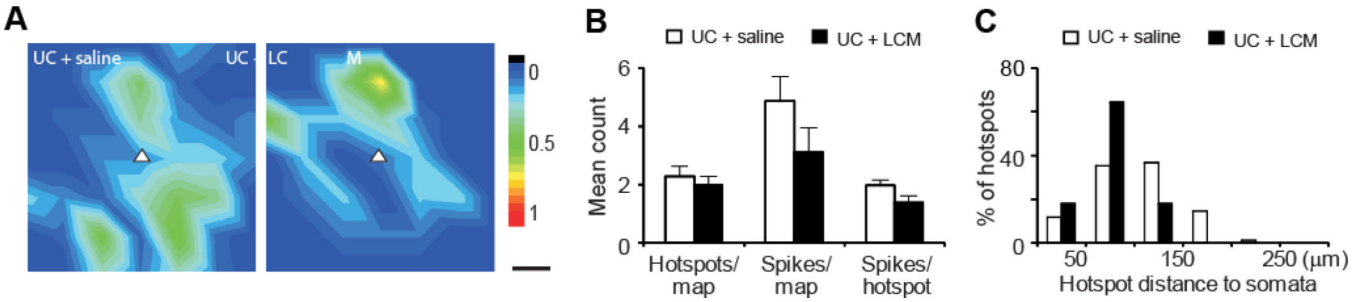

Figure 10. Similar direct excitation profiles of posttraumatic layer V pyramidal neurons in saline and LCM treatment groups

The purpose of this control experiment was to determine whether LCM treatment would change the responsiveness of pyramidal neurons to photostimulation. (**A, B**) Average uncaging evoked action potential (AP) maps in cortical pyramidal neurons have similar pattern and intensity in the two groups. White triangle: somata of recorded pyramidal neurons; color scale: mean number of APs evoked by photostimulation; black scale bar: 50 µm. (**B**) Comparisons in mean uncaging evoked hotspots per map, spikes per map, and spikes per hotspot between the two groups showed no significant differences between the two groups. (**C**) Distribution of hotspots relative to somata. Majority of uncaging evoked hotspots were located in areas about 100–150 µm from the somata in both groups.

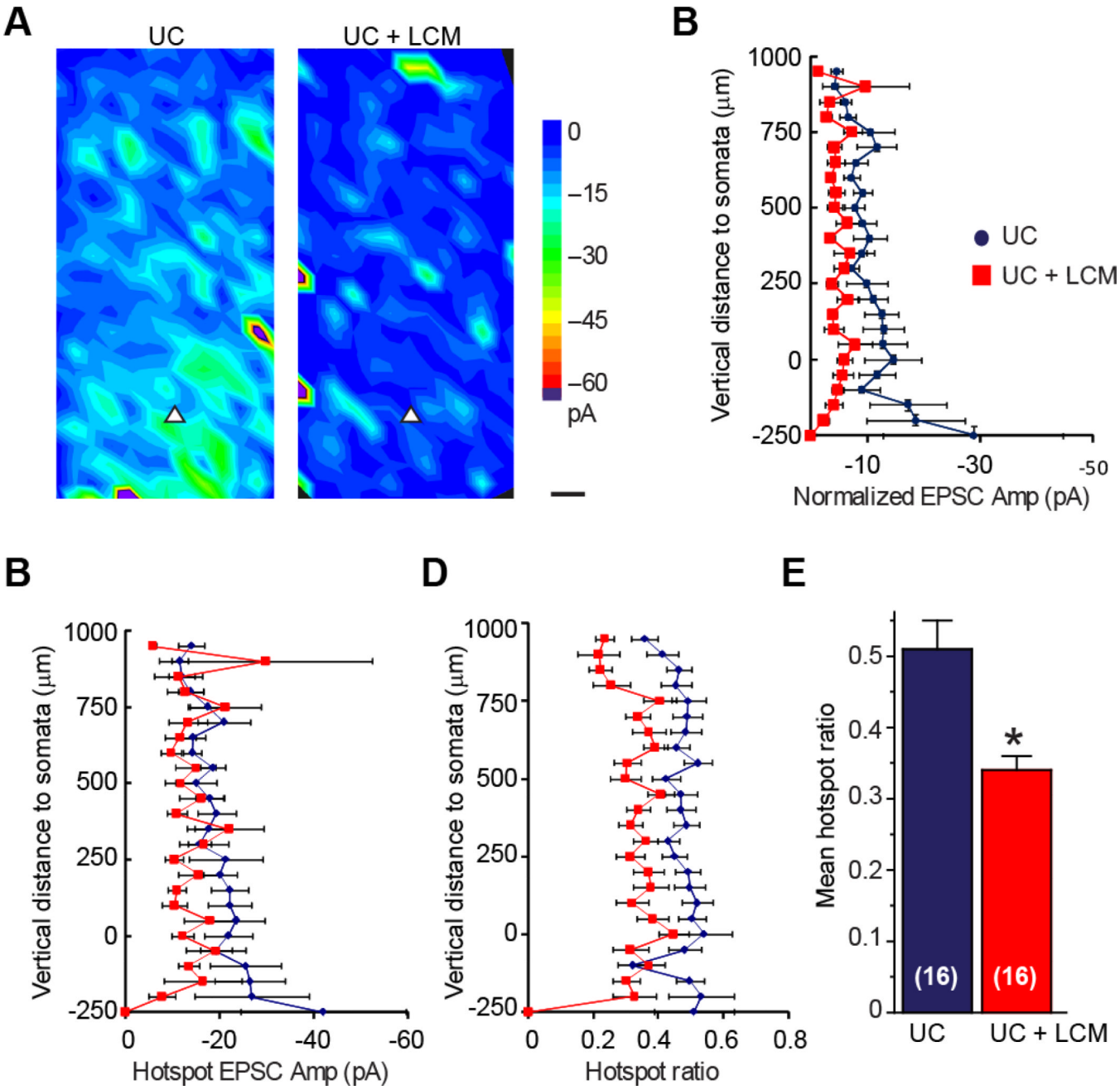

Figure 11. LCM treatment prevents the enhancement of excitatory synaptic connectivity after undercut injury

(**A, B**) Average uncaging evoked EPSC maps of layer V pyramidal neuron in the UC+saline (**A**) and UC+LCM (**B**) groups. Uncaging activated hotspots in average map of LCM treatment group were significantly less than that of the injured control group. Colar scale: composite amplitude of evoked EPSCs (pA); black scale bar: 50 μm. (**C–E**) Analysis of uncaging evoked EPSCs relative to the cortical depth. There was a significant difference between the two groups in hotspot ratio, but there were no significant differences between the two groups in normalized EPSC amplitude and hotspot EPSC amplitude. Zero position in the ordinate corresponds to the position of somata. Pial is toward the top of the graph,

white matter is towards the bottom. (**F**) Summary of mean hotspot ratio data from panel E. LCM treatment reduced overall hotspot ration ($P<0.05$, students *t*-test).